# Polymeric Nanoreactors for Intracellular Reactive Oxygen Species Production and Mimicking Cellular Environment

**Inauguraldissertation**

Zur

Erlangung der Würde eines Doktors der Philosophie

vorgelegt der

Philosophische-Naturwissenschaftlichen Fakultät

der Universität Basel

von

**Patric Michael Baumann**

Aus

Bern, BE

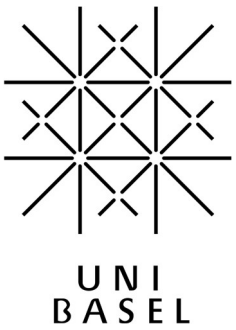


Basel, 2015

Genehmigt von der Philosophisch-Naturwissenschatlichen Fakultät

auf Antrag von

Prof. Dr. Wolfgang Meier (Universität Basel)

und

Prof. Dr. Marcus Textor (ETH Zürich)

Basel, den 24.03.2015

Prof. Dr. Jörg Schibler

(Dekan)

# Table of Content

## Impact of the work

Publications:

- M. Spulber, P. Baumann, J. Liu, C. Palivan
  Ceria Loaded Nanoreactors: a Nontoxic Superantioxidant System with High Stability and Efficacy
  Nanoscale, 2015, 7, 1411

- A. Car, P. Baumann, J. Duskey, M. Chami, N. Bruns, W. Meier
  ph-Responsive PDMS-b-PDMAEMA Micelles for Intracellular Anticancer Drug Delivery
  Biomacromolecules, 2014, 15, 3235

- P. Baumann, M. Spulber, I. Dinu, C. Palivan
  Cellular Trojan horse based polymer nanoreactors with light-sensitive activity
  Journal of Physical Chemistry B, 2014, 118, 9361

- T. Schuster, M. G. Nussbaumer, P. Baumann, N. Bruns, W. Meier, A. Car
  Polymeric Particulates for Subunit Vaccine Delivery
  Advances in Delivery Science and Technology, Springer, New York, 214

- M. Spulber, P. Baumann, S. Saxer, U. Pieles, W. Meier, N. Bruns
  Poly(N-vinylpyrrolidone)-poly(dimethylsiloxane)-based polymersome nanoreactors for laccase-catalyzed biotransformation
  Biomacromolecules, 2014, 15, 1469

- A. Zabara, R. Negrini, P. Baumann, O. Onaca-Fischer, R. Mezzenga
  Reconstitution of OmpF membrane protein on bended lipid bilayers: perforated hexagonal mesophases
  Chemical Communications, 2014, 50, 2642

- D. Vasquez, R. Milusheva, P. Baumann, D. Constantin, M. Chami, C. Palivan
  The amine content of PEGylated chitosan Bombyx mori nanoparticles acts as a trigger for protein delivery
  Langmuir, 2014, 30, 965

- S. Jagadeesan, V. Balasubramanian, P. Baumann, M. Neuburger, S. Häussinger, C. Palivan
  Water-soluble Co(III) complexes of substituted phenathrolines with cell selective anticancer activity.
  Inorganic Chemistry, 2013, 52, 12535

- P. Baumann, V. Balasubramanian, O. Onaca-Fischer, A. Sienkiewicz, C. Palivan
  Light- responsive polymer nanoreactors: a source of reactive oxygen species on demand
  Nanoscale, 2013, 5, 217

- P. Tanner, P. Baumann, R. Enea, O. Onaca, C. Palivan, W. Meier
  Polymeric Vesicles: From Drug Carriers to Nanoreactors and Artificial Organelles
  Accounts of Chemical Research, 2011, 10, 1039

- K. Renggli, P. Baumann, K. Langowska, O. Onaca, N. Bruns, W. Meier
  Selective and Responsive Nanoreactors
  Advanced Functional Materials, 2011, 21, 1241

- P. Baumann, P. Tanner, O. Onaca, C. Palivan, W. Meier
  Bio-Decorated Polymer Membranes: A new Approach in Diagnostic and Therapeutics
  Polymers, 2011, 3, 173

## Conference Talks

ACS Meeting, Dallas, US, 16-20.03.2014
"Stimulus-responsive polymer nanoreactors for efficient photodynamic therapy"

Nanoscience in the Snow, Kandersteg, Switzerland,29.31.01, 2014
"Polymeric nanoreactor for Theranostic Applications"

EPF 2013, Pisa, Italy, 16.-21.06 2013
"Stimulus-responsive polymer nanoreactor for efficient photodynamic therapy"

Swiss Soft Days XIII, Geneva, Switzerland, 1.06.2012
''Nanoreactors for *in situ* Photodynamic Therapy

NRP 62 Smart Materials: Annual Meeting, Fribourg, Switzerland, 15.-16.09.2011
Enzymatic cascade reaction in polymeric nanocontainer

NRP 62 Nanocontainer Meeting, Fribourg, Switzerland, 22.08.2011
Smart Nanoreactor Gate

**POSTER PRESENTATIONS:**

Soft control, Darmstadt, Germany, 22.-24.09.2013
A. Car, P. Baumann, N. Bruns, W. Meier
pH responsive polymersomes for drug delivery

SCS Fall Meeting, Lausanne, Switzerland, 6.09.2013
P. Baumann, M. Spulber, A. Sienkiewicz, C. Palivan
Polymer nanoreactors as an efficient source of radicals „on demand" for photodynamic therapy"
D. Wu, P. Baumann, M. Nussbaumer, C. Palivan, W. Meier
siRNA delivery system based on diblock polymer PMOXA-PBLA

PolyColl, Basel, Switzerland, 7.06.2013
A. Car, P.Baumann, N.Bruns, W. Meier
Towards pH-responsive polymersomes for cancer vaccine delivery
K. Langowska, P.Baumann, W. Meier
Polymeric nanoreactors for medical applications

Frontiers in polymer science, Sitges, Spain, 21.-23.05.2013
D. Vasquez, Y. Matter, P. Baumann, C. Palivan, W. Meier
pH responsive PEG-*b*-PMCL-*b*-PDMAEMA triblock copolymer for protein therapy

i-net Next Nanostar, Basel, Switzerland, 21.03.2013
P. Baumann, M. Spulber, W. Meier, C. Palivan
Efficient Photodynamic Therapy via Polymer Nanoreactors

Swiss Nanoconvention, Lausanne, Switzerland, 23.-24.05.2012
P. Baumann, V. Balasubramanian, O. Onaca-Fischer, A. Sienkiewicz, C. Palivan
Efficient Photodynamic Therapy *via Polymer* Nanoreactors

Swiss Soft Days III, Fribourg, Switzerland, 20.10.2010
P. Baumann, O. Onaca, C. Palivan, W. Meier
Protein gates allow *in situ* enzymatic reaction in polymer nanocompartments: Towards synthetic organelles

Frotiers in Chemistry, Paris, France, 21.5.2010
P. Baumann, O. Onaca, M. Meier
Bioconversion inside Nanoreactor

# 1. Motivation

Medicine is always searching for new ways to improve patients' conditions. The use of nanotechnology in medicine has recently opened a new field called "nanomedicine" which mainly aims to open new perspective of treatments and increasing therapeutic efficacy of existing therapies[1,2]. In the past years nanomedicine has gain attention all over the world and developed new approaches for medical treatments, as solubilization and targeting of cancer medicine or diagnostical tools. Different journals as "Nanomedicine – Nanotechnology, Biology and Medicine," "International Journal of Nanomedicine" or "Nanomedicine" exclusively publish articles related with nanomedical topics, while other journals have subchapters dealing with the topic and development of nanomedicine.

Nanomedicine generally describes the implementation and development of nanotechnology for medical applications[3]. It has a broad range of use, starting from solubilization of specific drug substances, to targeted-delivery systems in a body into a specific tissue or nanoelectronical sensors which are able to detect even the smallest quantities of desired molecules[4]. Nanomedicine aims to support and improve medicine by using properties of nanomaterials in order to diagnose or treat diseases at a molecular level[5]. Especially in cancer therapy nanomedicine has generated a lot of aspiration and visibility[6]. Nanomedicine for cancer therapy for example can improve the transport of a pharmaceutical active substances into the desired tissue, while decreasing the drug substances accumulation in non-target-tissue, additionally drug substances can be protected from degradation and cellular uptake is also facilitated[7]. Materials used for nanomedical approaches rang from natural lipids to modified proteins, antibodies or synthetic polymers. These materials are used to increase the efficacy of various treatments and therefore serve the patients well-being.

To understand therapeutics activities on a nanoscale level and to use nanoscale objects for improving current therapies we focused in this thesis on two different approaches:

i.) Encapsulation of a photoactive molecule in a polymersome to investigate its ability to be used in cancer therapy (Figure 1).

ii.) Encapsulation of an enzyme in a polymersome to study its activity under different crowding condition to mimic a cellular like environment.

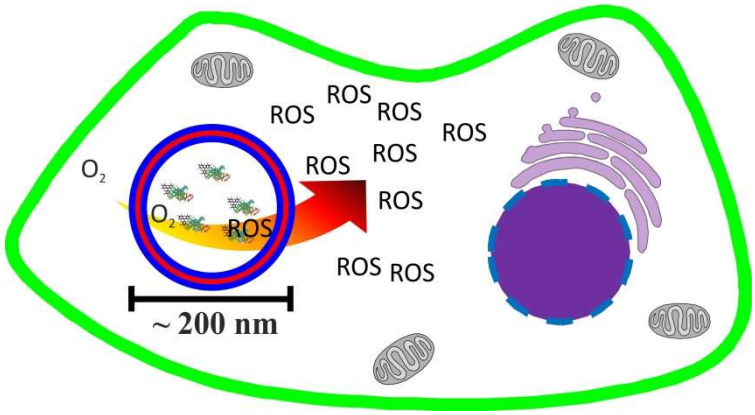


***Figure 1*** *Schematic illustration of the conceptual Trojan horse like nanoreactor acting upon illumination as a source of reactive oxygen species inside a cancer cell.*

## 1.1. Encapsulation of photoactive molecules in a polymersome to investigate its ability to be used in cancer therapy.

The classical method of nowadays cancer therapy are surgery, radiotherapy and chemotherapy. But cancer is still one of the main causes of death worldwide. A novel approach for cancer treatment is photodynamic therapy (PDT), which claims to be more precise and effective as the other methods. A real breakthrough in PDT was not achieved yet and a lot of hope is that nanomedicine can help to improve PDT in such a way that it can replace or support the classical methods.

We wanted to create a polymersome encapsulating a photodynamic active molecule in high amount to serve as source of reactive oxygen species (ROS) on demand. The amount of ROS produced with such polymersome should be high enough to induce cell death while illumination

with low light dose. Additionally the polymersome should be stable to stay intact while blood circulation and cellular uptake.

## 1.2. Encapsulation of an enzyme in a polymersome to study its activity under different crowding condition to mimic a cellular like environment

Many diseases are caused on a malfunction of a cellular receptor or a failure of an enzyme. To understand the interaction and activity of these biomolecule many parameters as the Michaelis-Menten constant are evaluated. The Michaelis-Menten constant which is reflecting the enzymatic activity is normally measured in optimized conditions for the enzymes which are not reflecting the real conditions they have to work on.

We wanted to encapsulate an enzyme into a polymersome to simulate a compartmentalized space. As enzymes are also working not in bulk but in a closed environment as a cell, the approach to measure enzyme activity in polymersome would be closer to the real activity of enzymes. Additionally to embrace the fact that the enzymes are surrounded by many macromolecules while performing their catalysis we want also to evaluate the effect of macromolecule in the presence of the enzyme. The combination of encapsulating and a crowded environment would give a tool to measure enzyme activity in an artificial cellular like environment.

# 2. Introduction

For both studies the use of a polymersome in the nanometer scale is essential to fulfill the set objectives. Polymersomes are artificial vesicles enclosing an aqueous cavity. They are formed by self-assembly of amphiphilic copolymers and can be produced in different sizes. Additionally, optimization on the vesicular membrane can help to adjust the polymersomes for different applications, *e.g.* as drug delivery vehicles or artificial organelle.

## 2.1. Polymers

Polymers are present in everyday life as of plastics such as polyethylene terephthalate (PET) in drinking bottles or polyethylene glycol (PEG) in shampoo or shower gel. Polymers are chemical compounds consisting of many repeating subunits called monomers, and they can exist as chains or in branched form. Besides synthetic polymers, natural polymers are essential in nature, as they are involved in different aspects of life on the molecular level. Deoxyribonucleic acid (DNA) and proteins for examples are two essential biopolymers and without them life would not exist in the form we know it. DNA and proteins consist of different subunits (monomers), while PET or PEG are built up of only on kind of monomer. Polymers consisting only of one type of repeating unit are called homopolymers, while polymers made from different building blocks are called copolymers. As polymers (homo and copolymer) are made up of typically more than ten repeating units and therefore have a high molecular weight, polymers are also classified as macromolecules.

## 2.2. Block Copolymers

Polymers that are used to form polymersomes are so called block copolymers and have an amphiphilic nature. A copolymer is a polymer resulting from more than one species of monomers[8] and can have a random order of the monomers. Block copolymers are macromolecules that contain different adjacent blocks of chemically distinctive monomers, different composition or different sequence distribution[9]. A block copolymer that consists of two types of monomers is called a diblock copolymer. When the block copolymer contains a hydrophobic (non-polar) and a

hydrophilic (polar) block it possess amphiphilic properties. Amphiphilic block copolymers can self-assemble in aqueous solution into various supramolecular structures as micelles, rods, nanoparticles or polymersomes[10,11]. Different diblock copolymers are currently employed for polymersome formation: Poly(ethylene glycol)-b-polyactide acid (PEG-PLA), poly(ethylene glycol)-b-poly(ε-caprolactone) (PEG-PCL), poly(2-methyl-2oxazoline)-b-poly(dimethylsiloxane) (PMOXA-PDMS), poly(acrylic acid)-b-poly(styrene) (PAA-PS) or poly(N-vinylpyrrolidone)-b-poly(dimethylsiloxane)-b-poly(N-vinylpyrrolidone) (PNVP-PDMS-PNVP)[12].

Triblock copolymers composed of an inner hydrophobic block attached to tow outer hydrophilic blocks are also used for polymersome formation. Examples of triblock copolymers used for polymersome formation are poly(2-methyl-2oxazoline)-b-poly(dimethylsiloxane)-b-poly(2-methyl-2-oxazoline) (PMOXA-PDMS-PMOXA), poly(N-vinylpyrrolidone)-b-poly(dimethylsiloxane)-b-poly(N-vinylpyrrolidone) (PNVP-PDMS-PNVP) or poly(oxyethylene)-b-poly(oxypropylene)-b-poly(oxyethylene) (PEO-PPO-PEO)[13].

In this work two different types of triblock copolymer were used: PMOXA-PDMS-PMOXA and PNVP-PDMS-PNVP. Both triblock copolymers are linear polymers of the type ABA, where A is a hydrophilic part and B a hydrophobic block.

PMOXA (the hydrophilic block) was shwon to be biocompatible and is mostly cleared from the blood stream after 24 h[14]. As degradation of PDMS in the body is slow, the clearance from the blood stream is linked to renal clearing. PDMS with lower molecular weight (around 5 kDa) can be removed from the body easily, while higher molecular weight PDMS has a tendency to accumulate in tissue[14]. The kidney has a molecular weight cut-off of approximately 30-50 kDa[15], which explains that smaller the polymers are, the better they get cleared from the body, even if they are not biodegradable. Additionally, an advantage of PMOXA is that it is protein repellent[16], which could be helpful for medical application to avoid an immune respond. Being protein repellent refers to the stealth properties of pegylated liposomes, which show better blood

circulation properties as non-pegylated[17]. The hydrophilic block of the polymer is in contact with the body fluids, PMOXA is preferred because of its non-ionic nature. In case of charged polymers the self-assembled polymersome could induce stronger immune response and therefore be less tolerable for medical applications. Additionally, it was shown that PMOXA can be used for medical applications[18,19] and by end-functionalization additional properties *e.g.* cell targeting, can be introduced on the surface of the nanoreactors[20].

PNVP, another hydrophilic polymer, shows low toxicity even at high concentration of up to 1000 µg/mL [21]. PNVP was used as hydrogel for drug delivery for controlled release of different drug substances and it is used as excipient in the pharmaceutical industry[21,22]. PNVP can also be used as solubilization agent, due to its high water solubility, which then can be used to conjugate for example to a tumor necrosis factor-α(TNF-α) and then apply it intravenous to mice[23]. The PNVP conjugated TNF-α had extended blood circulation time compared to PEG-TNF-α and a 90-fold higher plasma-life than native TNF-α, which proves the biocompetability of PNVP in animals.

PDMS, the hydrophobic block, which is used as constituent material for contact lenses or breast implants, is known to be biocompatible for a long time [24]. Due to the good ability to form PDMS with accuracy of few nanometers [25], it has also been used for life-saving devices like pacemakers and is well-known in the medical field. PDMS is used in food industry as anti-foaming agent as additive E900 in concentrations up to 10 mg/L, which shows the good tolerability of PDMS in humans. Additional silicon based polymers also have a good bio durability helping to improve stability of self-assembled structures made of PDMS. PDMS has a low glass transition temperature (Tg= 146 K), which makes the PDMS chain flexible at room temperature or higher [26]. Otherwise it is also stable under oxidative conditions and at higher temperatures, which partially explains the good chemical and biological stability [27-29].

The combination of one hydrophilic polymer (PMOXA and PNVP) with the hydrophobic PDMS allows to build an amphiphilic polymer, which can then be used for self-assembling nanomedical structures, since all of the polymers are known to be tolerable for medical applications.

## 2.3. Self-assembly of amphiphilic block copolymer

Amphiphilic block copolymers can, as already mentioned, self-assemble in aqueous solution into different structures. The obtained architecture is depending on several parameters such as concentration, molecular weight, geometry of the amphiphilic polymer or the ratio of the different blocks. The preferred structure we achieved to obtain are polymersomes and therefore the chosen triblock copolymers were optimized to form vesicular structures with an aqueous core.

A similar behavior can be observed if lipids – naturally amphiphilic molecules – were dissolved in aqueous solution. Liposomes (from lipids and the Greek word soma (body)) were normally formed in aqueous solution, which is also the case for their synthetic analogue: the block copolymers[30,31]

The self-assembly is mainly driven by non-covalent interaction (van der Waals forces) of the hydrophobic block. The aqueous phase favors the hydrophilic blocks and this triggers the self-assembly process to avoid water contact with the hydrophobic part of the block copolymer[32].

Polymersomes can be generated in different sizes, from tens of nm up to µm - so called giant polymersomes[33,34]. The size of polymersomes is influenced by different parameters from the amphiphilicity of the polymers themselves, up to the preparation methods used to self-assemble the polymersomes. After the formation of the polymersomes their structure can be additionally influenced by external effect such as extrusion, sonication or freeze/thaw cycles[35,36]. The thickness and fluidity of the membrane depends on the character of the block copolymer. The thickness of the polymersome membrane is influenced by the molecular weight and the block number (tri- or diblock)[37]. Triblock copolymers with the same molecular weight as diblock

copolymers are forming thinner membranes and the higher the molecular weight of a block copolymer is, the thicker is the polymersome membrane.

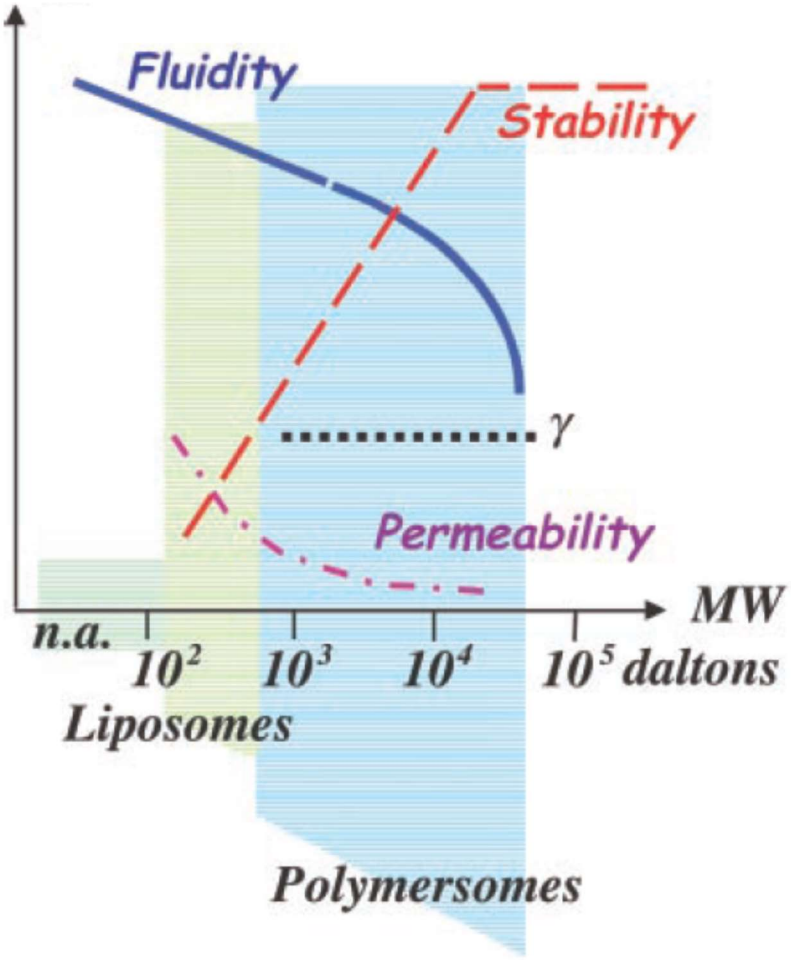


*Figure 2 Higher molecular weight of the building blocks of a polymersome lea to increase stability and lower permeability compared to liposome (reprinted with permission of [30])*

## 2.4. Nanoreactors

Polymersomes are usually employed for encapsulating of molecules. Further developments of polymersomes as nanoreactors, include the *in situ* production of active molecules. Nanoreactors combine the possibility to shield active molecules such as enzymes or proteins in nanometer size compartments, while preserving their functionality *in situ* [38].

## 2.5. Medical application of self-assembled structures

### 2.5.1. Polymersomes

Lipid based drug carriers are already approved for nanomedical purposes and in clinical trials and on the marked for several years. Examples for drug delivery system based on Liposomes are: Doxil, Visudyne, Thermodox or AmBisome[39-42]. Nowadays drug delivery systems are created by encapsulation of the drug substance in the aqueous core of a self-assembled structure[38]. The release of the drugs from the drug delivery system can be triggered by, pH, redox potential, light, magnetic field, differences in ionic strength or by instability of the system[12]. The advantages of higher stability of polymersomes over liposomes can be used to obtain more controlled release kinetics. Release that will start only after the delivery to the specific site would be an additional improvement of nanomedical fomulations. For example poly(butadiene-ethylene oxid) PB-PEO polymersomes were loaded with paclitaxel and they showed a steady release over 5 weeks at 37 °C, correlated with reduced cytotoxicity[43]. Therefore, a long term drug releasing system can be achieved by choosing the appropriate polymer system. This is helpful to maintain a constant concentration of drug in the blood or at the targeted tissue (the so called 'therapeutic window') for a long time, without the requirement of administration of further doses.

Fluorescently labeled poly(2-methacryloyloxyethyl phosphorylcholine)-poly(2-(diisopropylamino)ethyl methacrylate) (PMPC-PDPA) polymers were used for example for *in vivo* studies, because they preferentially accumulate in tumor tissue, which may enhance polymersome based cancer therapy [44]. The accumulation of a delivery cargo in tumor tissue is beneficial due to the reduction of the initial doses, related with lower side effects, as the drug is only released at the targeted site. Proper targeting and release of the active molecules in the desired location still needs to be improved for *in vitro* applications. Nevertheless, polymersomes have a broad range of biomedical applications in cancer therapy, diagnostics and vaccination[38].

### 2.5.2. Nanoreactors

Polymersomes are usually employed for targeted delivery of loaded active biomolecules. Further developments of polymersomes as nanoreactors, includ the *in situ* production of the desired active molecules. The greater stability of the nanoreactors compared to liposomes, is related to the polymer membrane and helps to maintain the encapsulated bio-active molecule inside the aqueous cavity and let the active molecule react in the presence of the substrate or when activated by an external trigger. To supply the bio-active molecule with starting materials for the reaction and to guarantee the escape of the newly formed molecules from the nanoreactor, a selective permeability of the nanoreactor membrane is required. Approaches to bring the bio-active molecule together with its substrate are i.) using a substrate-permeable polymeric membrane or ii.) inserting membrane proteins into the polymeric membrane allow efficiently exchange of molecule across the polymer membrane[45]. PNVP-PDMS-PNVP block copolymers as well as PMOXA-PDMS-PMOXA are permeable for reactive oxygen species [46,47], while PMOXA-PDMS-PMOXA is also able to reconstitute channel proteins as the outer membrane protein F (OmpF), the ferric hydroxamate uptake protein component A (FhuA), the receptor protein for the phage T6 and colicin K (Tsx) or the Aquaporin Z (AqpZ) to increase the permeability[48]. In all cases, small molecules can to be exchanged from the aqueous cavity of the nanoreactor to the nanoreactors environment and *vice versa*, while the bio-active molecule possesses a much higher molecular weight than the cut off of the channel protein cannot escape.

The function of the nanoreactor depends on the nature of encapsulated bio-active molecule. For example by choosing the encapsulated enzymes, the nanoreactors can be used either to produce antibiotics *in situ* [49] or to act as an artificial organelle [50]. Encapsulated photosensitizer can be used to generate a Trojan horse like nanoreactor for application in photodynamic therapy (PDT)[51].

## 2.6. Characterization methods for polymersome and nanoreactors

Due to their size in the nanometer range nanoreactors cannot be visualized and characterized with the classical optical methods. To obtain structural data from the nanoreactors and concentration of entrapped molecules different methods were used.

### 2.6.1. Light scattering

Light scattering (LS) uses the Brownian motion of particle in solution to determine their size. Small particles diffuse faster in solution compared to larger objects. To detect this motion a laser with constant intensity is used to illuminate the sample while at different angles changes in light intensity are measured. A small particle only causes a short change in intensity while a large particle causes a longer change. The fluctuation in light intensity over time can be fitted with an autocorrelation function and linked to a particle size. This kind of LS is also called dynamic LS. The particle radius which is determined by this technique is called radius of hydration.

Different shaped particles have a different scattering profile at changing angles. If the average light intensity is recorded at different angles also a prediction on the particle shape can be done. The radius obtained by this technique (static LS) is called radius of gyration (Rg). Rg is the quadratic mean distance of the objects' part from its center of mass. If both radii are correlating, then the measured object is of a vesicular structure [52]. For nanoreactor this means that they are round shaped and have an aqueous core.

### 2.6.2. Transmission electron microscope

Due to the limitation of light microscopy regarding sub-visible particles, another microscope was developed, which uses electrons instead of light, because they have a much shorter wavelength than photons. The rule of thumb say that the resolution is maximum have of the wavelength (Abbe-limit).With normal light the smallest resolution would be around 200 nm, which is not enough to detect nanoreactors in the size range of 100 nm. A transmission electron microscope (TEM) uses electrons intensities to image samples, which gives a much higher resolution. The optics of a TEM is not done with glass lenses but with magnetic lenses to focus the electron beam.

The obtained image is a density profile of the samples as the denser a material is, the less electron can pass through and gives a gray colored image. Due to the resolution TEM can be used for structural observation of nanoreactors, but not for encapsulated dyes or molecules.

### 2.6.3. Size exclusion chromatography

Size exclusion chromatography (SEC) is a technique to separate differently sized objects in solution. It is used in the purification of polymers or proteins. The solution is eluted through a stationary phase based on small porous beads based on polymers. Theses polymer beads have pores of different sizes, where particles can be temporarily absorbed (Figure 4). Smaller particles are absorbed longer than particles larger than the pores. Therefore particles which are larger than the pore size will elute together through the column. The smaller particles will elute later, which makes it possible to separate for example polymersomes from proteins.

In this process the biological activity of enzymes or protein will remain, as there is no chemical interaction between the stationary phase and the mobile phase. During this process, the samples gets diluted, which is the disadvantages of this process.

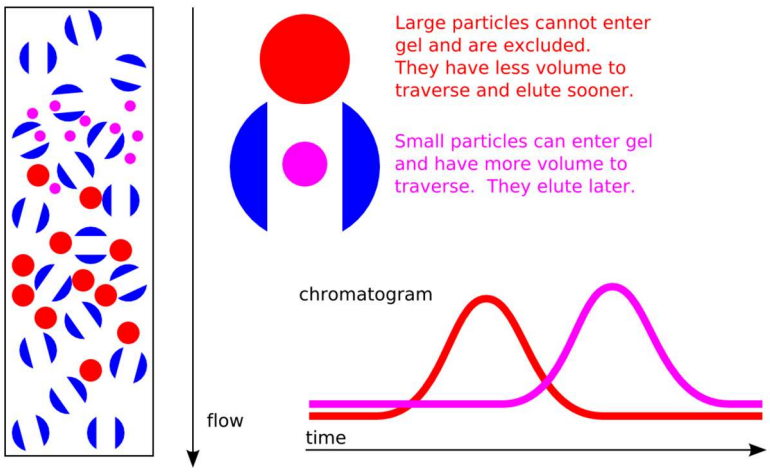


*Figure 3 Principle of size exclusion chromatography. Larger particles (e.g. polymersomes) will be separated from smaller objects (e.g. proteins) and will show up in the chromatogram at different time points[53].*

### 2.6.4. Spectroscopic methods

As the polymers used for nanoreactor formation are not absorbing in the visible light range, encapsulated molecules which are absorbing in the visible range can be detected spectrophotometrically. Concentration of dyes as rose Bengal can be determined using law of Lambert-Beer.

$$A = \varepsilon l c$$

Where A is the absorbance measured, ε is the extinction coefficient of the molecule, l the length of the pathway of the light and c the concentration of the measured molecule.

Due to the scattering properties (see light scattering) of large objects as the nanoreactors, a background correction by measuring empty nanoreactors is needed. From the absorbance of the nanoreactor containing a dye molecule the background can be subtracted and the concentration of the dye molecules can be calculated.

# 3. Polymeric nanoreactor to serve as Trojan horse for photodynamic therapy applications

Photodynamic therapy is a new approach to treat the leading cause of death in developed societies- cancer. The current most widespread clinical strategies to treat cancer patient are: i.) surgery, ii.) radiation therapy and iii.) chemotherapy[54]. Surgery is the fastest method but it has its drawbacks if the tumor is located close to a sensitive area or if the tumor has already formed metastasis no complete treatment can be achived. Radiotherapy on the other hand, damages DNA, but leaks selectivity and therefore damage healthy neighboring cells or tissue.

Chemotherapy suppresses cell growth or kills quickly dividing cells within the body. As a chemotherapeutic agents are distributed normally throughout the whole body undesired toxic side effects appear with this therapy, although the approach is advantageous in case of metastasized tumors.

In the past few years, the efficacy of chemotherapeutic agents has been improved by formulating them within nanocarriers, which improve the circulation time in the blood, by preventing renal clearance and non-specific uptake[54]. Additionally, an increased and targeted uptake into tumor tissue can be achieved by the enhanced permeability and retention effect (EPR).

## 3.1. Enhanced permeability and retention (EPR) effect

EPR - relies on the ability of tumor cells to grow faster and therefore on the fact that these cells require more nutrients and oxygen. Consequently the new formed blood vessels in tumor tissues show defects and larger openings that can allow the passage of structures with size around 200 nm compared to healthy blood vessel[7]. Therefore nano-sized structures such as liposomes, polymersomes or micelles are favored in drug delivery by taking advantages of the EPR effect. Due to their size, these nanoparticles accumulate preferentially in the tumor tissue, while smaller molecules and larger assemblies do not profit from this size selection. The selectivity is only generated by the size and does not need an additional active targeting to the tissue.

The selectivity is a crucial point of the treatment, as the more selective a treatment is, the less side effects can occur. Therefore novel methods for more selective treatment have been developed to fight cancer and improve patient's conditions. To this point, photodynamic therapy (PDT) is a promising strategy as is has a dual selectivity, based on a photosensitizer exposed to light. Furthermore, the combination of nanomedicine with PDT even increases the selectivity of the therapy.

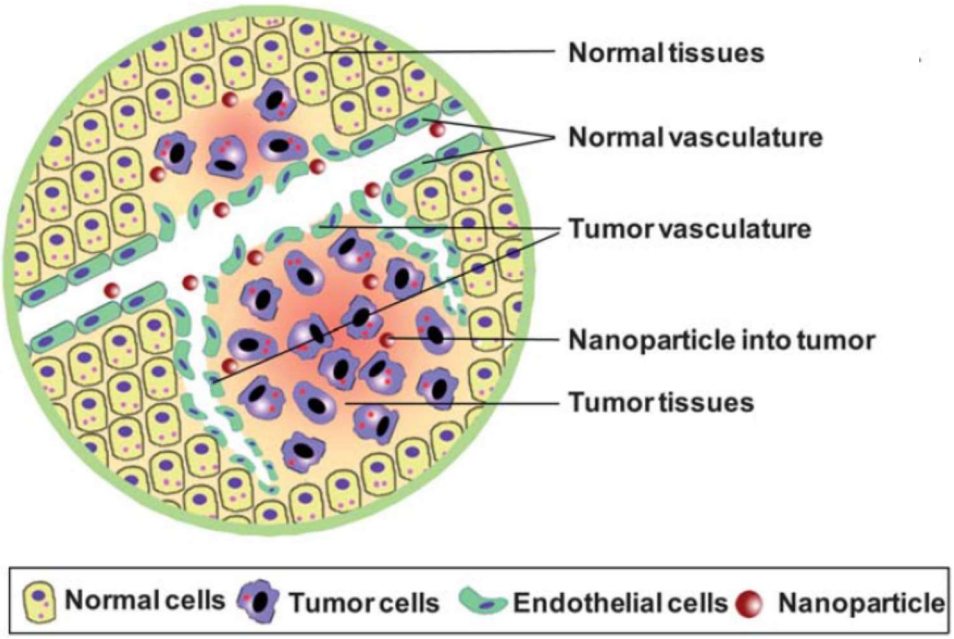


*Figure 4 Principle of the enhanced permeability and retention effect (EPR), where in tumor tissues the endothelia cells of the blood vessels are less densely packed as in healthy tissues, which allows particles around 200 nm to diffuse easily into tumor tissue (reprinted with permission of [7]) .*

## 3.2. Photodynamic therapy (PDT)

PDT uses the ability of excited photosensitizer to transfer energy to molecular oxygen returning to the unexcited state[55-58]. In this way molecular oxygen, is converted to ROS (cytotoxic reactive oxygen radicals) which will induce - apoptosis and cell death. Compared with classical chemotherapy PDT has the advantage of a photosensitizer that has normally minimal toxic effect in the absence of light, even if accumulated in non-specific tissues[54]. Additionally due to the low toxic side-effects of PDT, PDT needs an external trigger (light) to be activated and therapy can be repeated as needed.

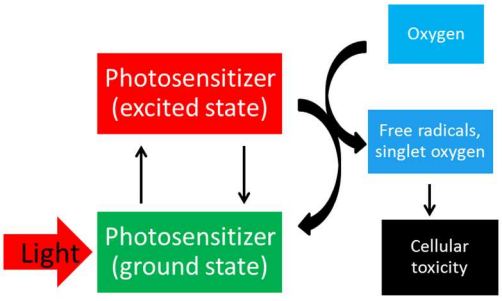


***Figure 5*** *Photodynamic therapy needs three components (light, photosensitizer and oxygen). Light can activate from the ground state to an excited state a photosensitizer at a specific wavelength of light. The energy can be transferred to oxygen, which is than transformed into reactive oxygen species, which lead to cellular toxicity.*

To date, only few PDT based therapy formulations have been marked (*e.g.* Photofrin® Visudyne® or Foscan®). PDT is limited with respect of targeting and penetration depth. UV light has a maximum penetration depth of 1 mm, while a wavelength of 630 nm can reach a maximum depth of 6 mm into the skin[59]. Therefore most of the marked PDT treatments are used in skin cancer therapy, when the tumor tissue is not large and easily accessible to light.

Properly delivered and activated photosensitizer can cause all three forms of cell death (apoptosis, necrosis, and autophagy). Photosensitizer can act on different organelles, such as mitochondria, endoplasmatic reticulum, Golgi apparatus or directly on the plasma membrane[60]. The stimulated production of reactive oxygen species lead to an increase of the oxidative stress that will induce the oxidation of enzymes and interruption of repair mechanisms, which ends in cell activated apoptosis[60]. The cellular response will be influenced by several different factors, such as photosensitizer, localization, experimental model and light dose to induce multiple metabolic changes and cell death mechanism.

The drawback of current photosensitizers is that most of them are hydrophobic and had to be formulated for administration so that the photosensitizer reaches the target tissue[61]. The help of nanomedicine can help to overcome this problem and may even use the EPR effect for passive targeting[7,62]. Additionally, drug delivery systems normally have the advantages of causing lower side-effects. Nanomedicine drug delivery system can also be compared with the legendary Trojan

horse, with which the Greek soldiers were delivered into the city walls of Troy, buried a huge wooden structure. A more modern Trojan horse is a computer virus embedded within a friendly looking program. The design of a Trojan horse for PDT has to be stable at least till it is delivered into the cells and be activated upon arrival[51] [Baumann_2013].

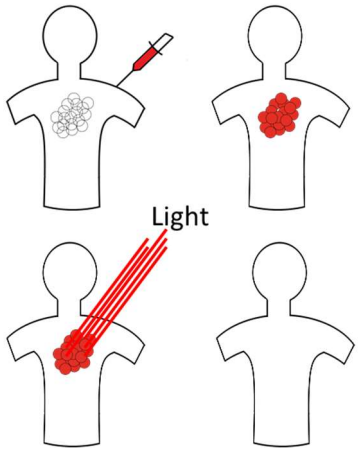


***Figure 6*** *Photodynamic therapy is used for targeted cancer therapy; thereby the formulated photosensitizer is injected into the patient and delivered to the tumor tissue. Activated by external light the produced ROS is selectively destroys the tumor tissue.*

## 3.4. Conjugation of photosensitizer with bovin serum albumin (BSA)

For the photodynamic therapy experiments Rose Bengal (RB) was chosen as photosensitizer, due to the high photodynamic activity, good quantum yield, absorption in the visible region, and inexpensiveness[63,64]. The high quantum yield of Rose Bengal helps to keep the amount of photosensitizer low. But on the other side Rose Bengal has a tendency to interact with the polymeric membrane so in order to avoid this kind of interaction the solubilization of RB was tried in such a way its efficacy was maintained.

A method to increase the solubility of RB without any chemical modification is conjugation with bovine serum albumin (BSA). Additionally the conjugation to a protein will help to avoid interaction of the photosensitizer with the polymersome membrane, as PMOXA – the hydrophilic part of the nanoreactor membrane – is protein-repellent. If no interactions between the membrane and the photosensitizer happen the system can be better controlled in terms of

stability and purity. The conjugation between RB and BSA is known to be a stable hydrophobic interaction[65], leading to a shift in the maximum absorbance of RB from λ=547 nm to λ=559 nm (see figure 4) [66]. Depending on the ratio of RB to BSA the maximum absorbance peak can vary between these values, while higher BSA content leads to red-shifted of spectra. An optimal ratio of RB to BSA was found to be 1:1, while for the experiments a small excess of BSA was used, which should guarantee that no free RB is present in the stock solution used for encapsulation. With the use of BSA another problem appeared. Higher concentration of BSA can influence the self-assembly process and therefore a maximum concentration of BSA (10 mg/mL) was found to be the upper limit. At this concentration the self-assembly process of the nanoreactors was not affected.

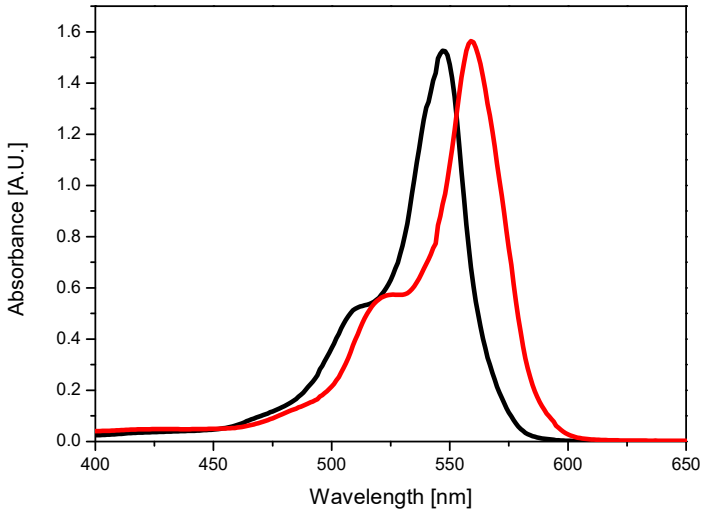


***Figure 4*** *UV-Vis spectrum of rose Bengal (black line), and rose Bengal-BSA conjugates after purification with a HI-Trap column (red line) in PBS buffer at room temperature.*

## 3.5. Polymer synthesis

The used PMOXA-PDMS-PMOXA polymers were synthesized by a polycondensation reaction of PDMS monomers followed by a cationic ring opening polymerization with 2-methyl-2-oxazoline

previously described by Meier et al. [67]. A final quenching of the reaction with KOH solution in methanol led to a hydroxyl-terminated triblock-copolymer.

From the $^{1}H$ NMR, the integrated peaks could be used to determine the composition of the triblock polymer, giving the different block length of the PMOXA and PDMS blocks. The obtained triblock polymer characteristics are presented in table 1.

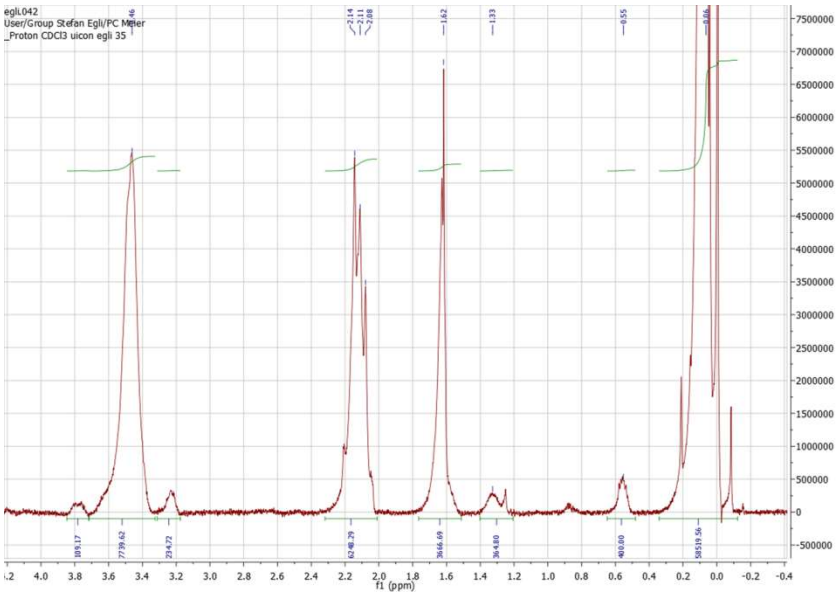


***Figure 5*** *$^{1}H$-NMR spectrum of PMOXA10-PDMS87-PMOXA10 polymer.*

The synthesis of PNVP-PDMS-PNVP polymer was performed according with the method already described in the literature by Simionescu and co-workers[68]. The resulting block length of the polymer are presented in table 1

***Table 1*** *Triblock copolymer used for the encapsulation of RB-BSA. The polymers were chosen, as these kinds of polymers are known to be permeable for ROS [REF].*

| Polymer name | Composition | Mn /(GPC) | reference |
|---|---|---|---|
| A1 | $PMOXA_{10}$-$PDMS_{87}$-$PMOXA_{10}$ | 8352 | [20] |
| A2 | $PMOXA_{14}$-$PDMS_{33}$-$PMOXA_{14}$ | 4720 | Polymer source P3691A |

| | | | |
|---|---|---|---|
| A3 | $PMOXA_6$-$PDMS_{44}$-$PMOXA_6$ | 4555 | [69] |
| B1 | $PNVP_{11}$-$PDMS_{17}$-$PNVP_{11}$ | 2360 | [47] |
| B2 | $PNVP_{17}$-$PDMS_{17}$-$PNVP_{17}$ | 4200 | [47] |
| B3 | $PNVP_{30}$-$PDMS_{37}$-$PNVP_{30}$ | 6160 | [47] |

## 3.6. Formation of polymeric vesicles

Polymersomes can be prepared in a similar way as the lipid analogues, the liposomes. Three main techniques can be used: i.) direct dissolving, ii.) co-solvent method and iii.) film rehydration. If a polymer is directly dissolved in aqueous media without any pre-treating, then this method is called direct dissolving. Depending on the hydrophobic properties of the polymers, not all polymers can be used for the direct dissolving method, as some of the polymers only swell but do not reassemble into a more complex architecture such as polymersomes.

The co-solvent method is performed by dissolving the polymer in a small amount of solvent (*e.g.* EtOH) and then adding it drop-wise to an aqueous solution under stirring. The added solvent can be removed after self-assembly by evaporation.

The optimal method to form polymersome was in our case the film rehydration method [51]. In a first step the block-copolymer is dissolved in an organic phase (*e.g.* EtOH) that is removed under reduced pressure. Due to the slow removal of the organic phase a thin film of the polymer is formed on the bottom of the flask, which increases the surface for rehydration of the polymer.

Finally the rehydration of the polymeric film was performed by adding the desired molecule aqueous solution and stirring. The speed of stirring was adjusted so that the stirring bar did not come in contact with air so as to avoid bringing oxygen into the system, which could lead to oxidation of the active molecule and therefore to a reduced activity of the nanoreactor. In order to help the mechanical detachment of the polymeric film the glass flask was tilted manually, so that the stir bar came into contact with the whole polymer film. The self-assembly process was normally done overnight at room temperature.

## 3.7. Encapsulation of RB-BSA into polymersomes

To produce a nanoreactor permeable to reactive oxygen species (ROS) different triblock copolymers were used. Both, PMOXA-PDMS-PMOXA and PNVP-PDMS-PNVP polymers were chosen due to their known permeability to ROS[47,70]. Different block lengths of the polymer were used (see table 1) to obtain a nanoreactor optimized from encapsulation efficiency and uptake behavior into cancer cells.

The nanoreactors were prepared by the film rehydration method at room temperature overnight under darkness. The preparation in the dark was to preserve the stability of the photoactive RB-BSA conjugate. As the film rehydration led to a large size distribution of polymersome, the nanoreactors were extruded several times through 0.2 µm filters, to obtain a narrow size distribution of the nanoreactors. Additionally smaller vesicles are known to support the enhanced permeability and retention effect[7]. This effect could help in further studies targeting tumor tissue, without further modification of the nanoreactor.

As the encapsulation is a statistical process, not all active molecules will be encapsulated during the film rehydration. In order to remove free RB-BS, size exclusion chromatography was used. The chosen size exclusion chromatography (SEC) gel (Sepharose 2B) is optimal to separate proteins such as BSA. The separation was detected with a UV-detector at the end of the column and the obtained chromatogram showed two separate peaks: one for free and one for encapsulated RB-BSA (See figure 6 A).

A sample of purified nanoreactors was applied on a SDS-PAGE and no free BSA was detected. This proved additionally that no interaction between the polymer membrane and the RB-BSA conjugate occurred, as empty nanoreactors were incubated as a control for one hour with RB-BSA at room temperature. After that chromatographic separation of the nanoreactors fractions was performed by SEC - no RB-BSA could be detected after separation indicating that RB-BSA does not attach on the surface of polymersomes.

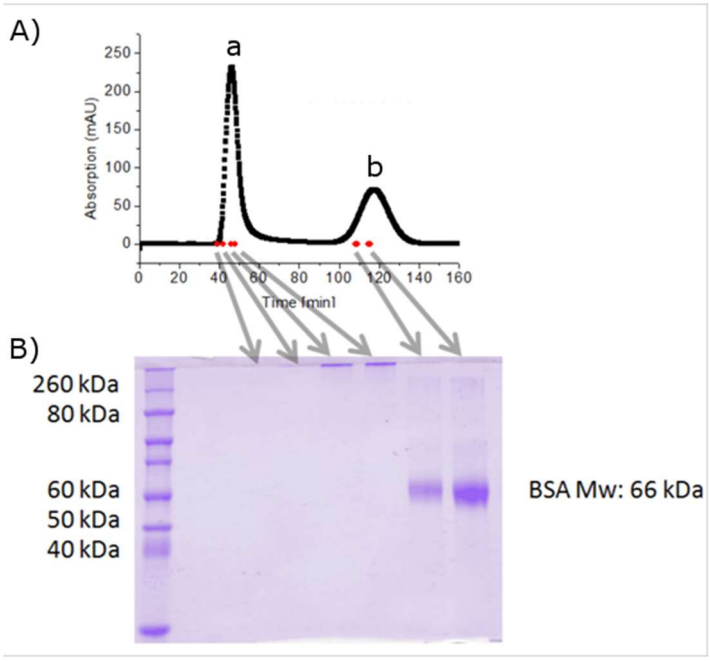


***Figure 6*** *UV (280 nm) chromatogram of the process that separates RB-BSA nanoreactors (a), and non-encapsulated RB-BSA (b). B) SDS PAGE of the fractions corresponding to Figure S2 A).*

The influence of encapsulation on the absorbance behavior was investigated by using the fluorescence properties of RB, which is also present in the conjugated form. While the non-conjugated RB has an emission maximum of 563 nm if excited with 543 nm light the conjugated form has an emission maximum around 578 nm (see figure 7). The presence of polymer vesicles does not influence the fluorescence emission spectrum of RB-BSA, even if encapsulated. This indicates that the polymer membrane is not a barrier for the light and will not limit the efficiency of the photodynamic activity of the nanoreactors.

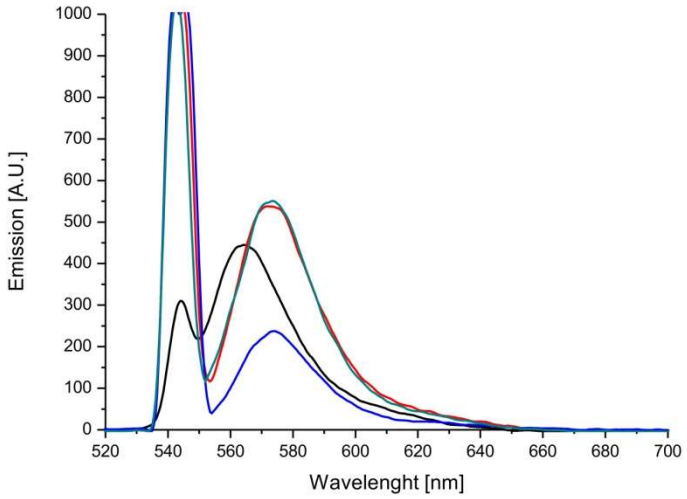


***Figure 7*** *Emission spectra of RB (black line), RB-BSA conjugate (red line), empty vesicles in presence of RB-BSA (green line) and nanoreactors with RB-BSA inside (blue line) measured in PBS buffer (excitation at 543 nm).*

## 3.8. Nanoreactors characterization

Purified nanoreactors were characterized from their encapsulation efficiency and size. Additionally, transmission electron microscopy (TEM) images were taken to confirm their morphology and size.

### 3.8.1. Encapsulation efficiency

To assess the encapsulation efficiency of the nanoreactors the maximum absorbance (λ= 559 nm) of a dilution series of known RB-BSA concentrations was measured spectrophotometrically and compared with the nanoreactors encapsulating RB-BSA after purification. Due to the scattering of the polymersome itself at this wavelength, spectra ranging from 400 nm to 600 nm were recorded and background correction was done. The background correction was defined for each measurement separately. With this method we ensured that the influence of the polymersome scattering was negligible. In order to estimate the encapsulation efficiency the amount in percent of the initial RB-BSA concentration was taken and additionally the dilution-factor was applied. Encapsulation efficiencies of 1.5 % to 13 % for different polymers were obtained (see table 2).

These values are similar to other polymersomes encapsulation proteins with comparable molecular weights[49,71].

### 3.8.2. Light scattering

Using static and dynamic light scattering the radius of gyration ($R_g$) and the radius of hydration ($R_h$) of the nanoreactors were determined. As the nanoreactors were extruded through a 0.2 µm filter membrane the expected radii were around 100 nm. With radii ($R_g$) ranging from 103 nm to 149 nm, the results are all above the expected value. Probably due to a slight deformation of the polymer membrane. The same behavior was observed by extruding the A1 polymer through smaller pores (0.1 µm and 0.05 µm). The discrepancy between the pore size of the filters and the measured size is larger the smaller the pore is. As the polymer membrane has a thickness of approximately 14 nm and a certain curvature of the membrane, the nanoreactors are more stable around 200 nm.

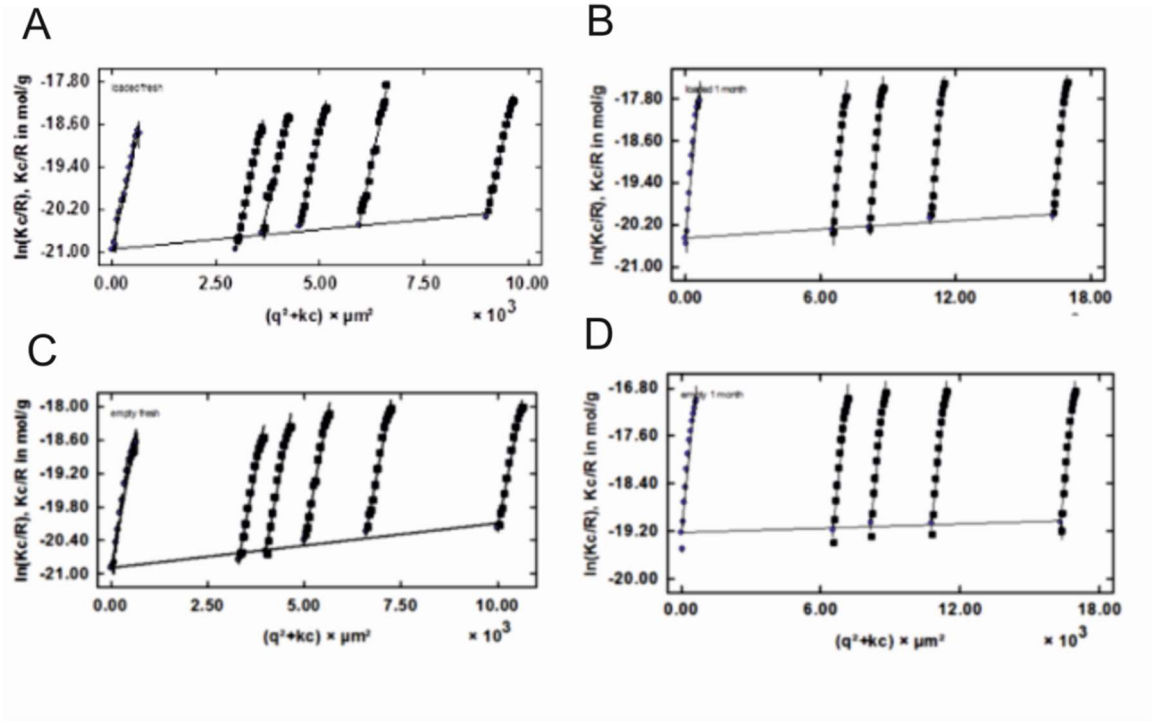


***Figure 8*** *Static light scattering Gunier plots of A1 nanoreactors: A) freshly prepared RB-BSA nanoreactors, B) RB-BSA nanoreactors after one month, C) freshly prepared empty vesicles, and D) empty vesicles after one month.*

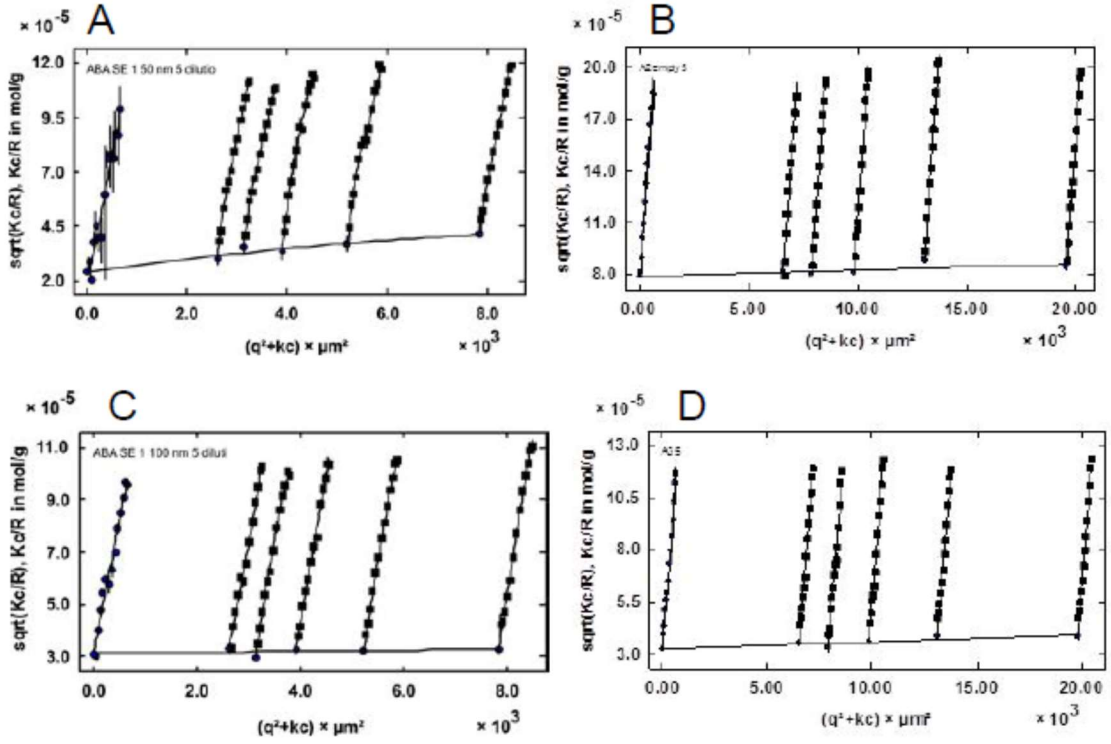


***Figure 9*** *Berry-Plots of (a) A1-50- (b) A1-100- (c) A2- and (d) A3- nanoreactors without illumination*

The ratio of both radii ($R_g/R_h$), if equal to 1, indicates a the formation of hollow spherical structures[52]. Additionally the second virial coefficient ($A_2$) is almost zero, indicating that no long-range interaction in the measured concentration range occured.

The obtained data for the $R_g$ and $R_h$ are comparable between nanoreactors with and without encapsulated RB-BSA (see table 2). The differences were within the error range of the measurement. Illumination with light did not induced changes in the morphology of the nanoreactors, which support their used for medical applications. Similar PMOXA-PDMS-PMOXA vesicles were also stable over several hours in blood plasma[72], which makes them also suitable for *in vivo* application.

***Table 2*** *Nanoreactor characteristics: Rg and Rh were determined using dynamic and static light scattering. The encapsulation efficiency was a results of absorbance measurement of the purified nanoreactors compared to the unpurified nanoreactors. RB-BSA conjugates per vesicles is based on a mathematic model (see materials and methods), to give ab impression of the amount of photosensitizer per nanoreactor.*

| Sample name | $R_g$ [nm] | $R_h$ [nm] | Encapsulation efficiency [%] | RB-BSA conjugates per vesicles |
|---|---|---|---|---|
| A1-200 | 103 | 109 | 13.0 | 22 |
| A1-100 | 70 | 74 | 13.0 | 7 |
| A1-50 | 55 | 60 | 13.0 | 4 |
| A1-200 empty | 107 | 112 | -- | -- |
| A2 | 89 | 95 | 2.3 | 2 |
| A3 | 149 | 157 | 12.5 | 61 |
| B1 | 120 | 118 | 1.5 | 3 |
| B2 | 112 | 121 | 3.8 | 13 |
| B3 | 118 | 129 | 8.6 | 23 |

### 3.8.3. Transmission electron microscopy (TEM)

In order to characterize the morphology of the formed self-assembled structures TEM was used. To induce a better contrast, before TEM measurements the samples were negatively stained with uranyl acetate.

On TEM micrographs collapsed spherical objects are visible, similar with those also observed by atomic force microscopy (AFM)[73]. The sizes of the collapsed structures are around 200 nm as shown by light scattering. The nanoreactors are separated from each other, which supports that no long-range interaction between nanoreactors can be seen.

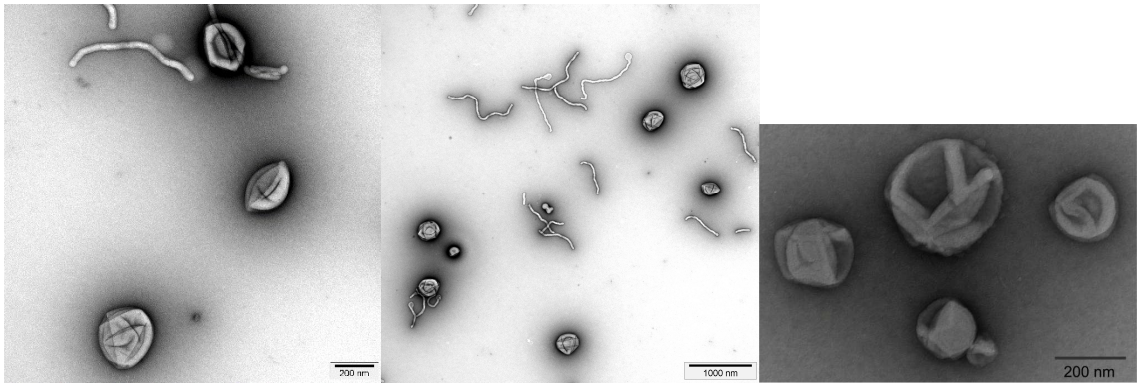


***Figure 10*** *A and B) ABA-1 nanoreactors after 200 nm extrusion, showing the usual collapsed spherical structure. Besides the formed nanoreactors also a few worm like micelles were formed, but due to their size they probably have not contributed to the encapsulation of RB-BSA. C) A3 micrograph of A3 nanoreactors with encapsulated RB-BSA.*

## 3.9. Nanoreactor activity

In order to quantify the ability of the nanoreactors to produce ROS under illumination a scavenger system for radicals was used. The scavenging molecules 2,2,6,6-tetramethyl-4-piperidinol (TMP–OH) and 5,5-dimethyl-1-pyrroline *N*-oxide (DMPO) were used to trap species produced by the photo-activity of rose Bengal and RB-BSA. The spin trap TMP-OH is a diamagnetic molecule and therefore not detectable with electron spin resonance (ESR). If reacted with reactive oxygen species it will be transformed into a paramagnetic molecule 4-hydroxy-2,2,6,6-teramethyl piperidin-1-hydroxyl (TEMPOL), detectable by ESR. As the nanoreactors are impermeable to most molecules except ROS the scavenger molecule cannot enter inside the nanoreactor. Therefore the radicals detected are the ones which cross the membrane of the nanoreactors and are of therapeutic value.

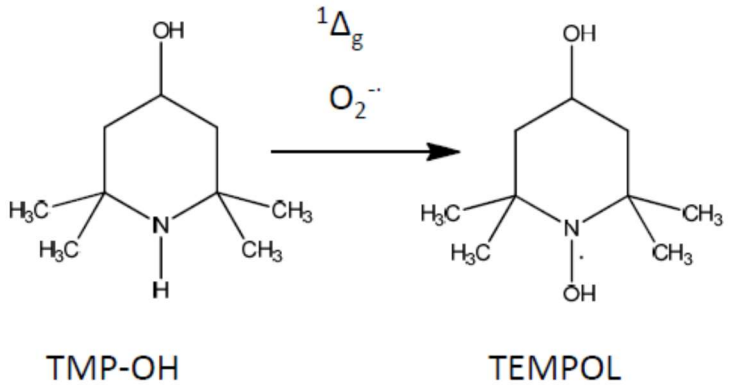


TMP-OH TEMPOL

***Figure 11*** *2,2,6,6-tetramethyl-4-piperidinol (TMP–OH) is acting as a spin trap and will be transformed in the presence of radicals and singlet oxygen to 4-hydroxy-2,2,6,6-teramethyl piperidin-1-hydroxyl (TEMPOL). As TMP-OH is ESR inactive (not paramagnetic) the new formed product TEMPOL is paramagnetic and can be easily be detected via ESR.*

The ability to produce ROS is dependent on the quantum yield of RB. The conjugated BSA and the shift in the absorbance could have an influence on the quantum yield. Studies on the photo activity by conjugating RB to peptides show no significant loss of photo activity[65].

To compare the activity of RB and the BSA conjugated RB, two solutions with both the same concentration of RB were mixed with the scavenging molecule and then illuminated with artificial daylight. After 0 min, 5 min, 10 min 15 min and 20 min the concentration of the formed ESR active molecule was measured.

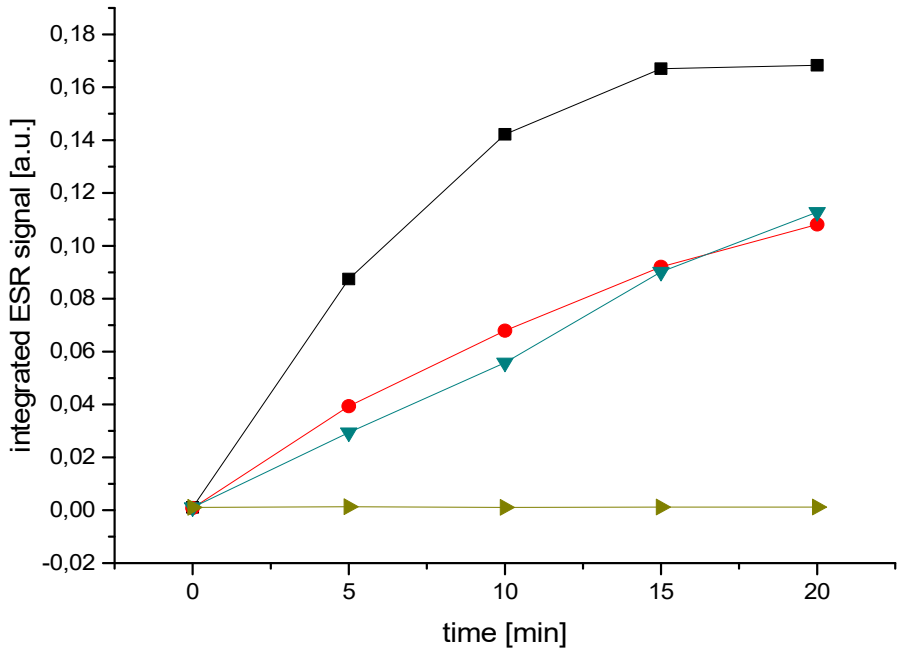


***Figure 12*** *Development of the integrated ESR signal while illumination with withe light. ■ (black) Increasing signal of formed ESR active TEMPOL in the presence of illuminated RB. ● (red) detected signal of the same concentration of RB but conjugated to BSA. ▼ (green) ESR signal development of RB-BSA encapsulated in A1-200 polymersomes adjusting the overall concentration of RB-BSA to the free condition. ► (olive green) Control experiment using empty nanoreactors in the presence of TMP-OH and light.*

For pure RB the signal of the spin trap increased faster than for the conjugate. At the end the RB-BSA conjugate showed about 70 % of the photo activity of pure RB in PBS buffer. The loss of activity can be explained by the red shift and the large BSA molecule conjugated to RB. The red shift implies a lower energy that can be absorbed by RB, which can influence the photo activity. Moreover, additional BSA conjugated to RB can absorb some of the produced ROS and therefore influence the measured activity. Nevertheless, due to the initial high photo activity of RB-BSA even 70% of its total activity could be expected to be high enough for photodynamic therapy.

As encapsulation of RB-BSA in nanoreactors was found to lower activity, both free and conjugated RB containing the same RB concentration encapsulated into nanoreactors were mixed with the spin trap and further illuminated. No difference between free and RB-BSA conjugated encapsulated in nanoreactors was observed. As the polymeric PMOXA-PDMS-PMOXA membrane

is known to be permeable to ROS the encapsulation had no effect on the photoactivity. As empty nanoreactors do not absorb light around 550 nm – 560 nm the full energy of the light can be transferred to the RB-BSA conjugate.

To investigate the nature of obtained ROS species the obtained signal was simulated and was shown to be composed by the contribution of a signal characteristic for TMP-OH was TEMPOL (g = 2.0055, $a_N$ = 17.13 G). – and a small fraction of 4-oxo-2,2,6,6-teramethyl piperidin-1-oxyl (TEMPONE) (g = 2.0054, $a_N$ = 16.13 G) due to the attack of $O^{2-}$ on TEMPOL. This suggests that different ROS molecules are produced in the nanoreactors and are able to diffuse out from there. As by conjugation and encapsulation in nanoreactors only 30% of RB activity was lost comparing to pure RB, encapsulated RB-BSA seems to be an interesting candidate for photodynamic therapy treatment.

## 3.10. Cytotoxicity of RB-BSA containing nanoreactors

To prove the biological compatibility and quantify the influence of nanoreactors on cell viability, HeLa cells were incubated with RB-BSA containing nanoreactors. HeLa cells are culturable cervical cancer cells that are well established in basic research[74]. Due to their fast growing and unspecific nature they are ideal for a first indication of cytotoxic effect of the nanoreactors. The toxicity was assessed by incubating HeLa cells with RB-BSA nanoreactors for 24 h. Different concentrations of A1-200 nanoreactors were incubated with HeLa cells and their viability was measured after 24 h with a 3-(4,5-dimethylthiazol-2-yl)-5-(3-carboxymethoxyphenyl)-2-(4-sulfophenyl)-2H-tetrazolium (MTS) assay. To avoid the production of ROS, which can maybe influence the viability results, the nanoreactors the manipulation of the cell culture was done in the dark. Surprisingly empty and loaded nanoreactors shows similar viability data, indicating that small doses of light did not induce cell death. The viability of the cells remained above 90 % up to a polymer concentration of 300 µg/mL, which considered a high dose in photodynamic therapy. The good biocompatibility is in agreement with other viability tests of similar nanoreactors.

RB is known to be toxic and therefore not extensively evaluated as a photosensitizer [75]. But as RB-BSA is only encapsulated in the nanoreactor and not attached on the membrane it was not expected to add any additional toxicity. The low toxicity observed can be obtained from inhibition of growing of the cells and RB-BSA induced. This also clearly indicates that the encapsulation in nanoreactors prevent toxicity based on RB-BSA.

## 3.11. Cellular uptake studies

It is important for the efficiency of photodynamic therapy that it is active *in vitro* and not only *in situ*. To be an efficient system, the nanoreactor has to be able to enter into the cells, as inside the cell the damage generated by ROS have a higher impact than in bulk. Therefore the uptake into cells without degradation or damage of the photosensitizer is an essential step for the action of the nanoreactor.

In order to assess the ability of nanoreactor to be taken up by cells the fluorescence property of RB was used. RB is slightly fluorescent[76,77] and can be excited with a 543 nm laser and detected by flow cytometry and fluorescent microscopy.

To prepare cells for uptake experiments they were first cultured for 24 h without nanoreactors. Nanoreactors were then added and the cells were cultured for an additional 24 h. Nanoreactors were not sterilized any further for use, as they were already extruded through 0.2 µm filters. An additional sterilization step was avoided as it could also have induced changes in the structure of the nanoreactors or affect their integrity.

To investigate if the nanoreactors were taken up by the cell and not just attached to the cellular surface, cells were washed before the experimental read-out several times with PBS to remove nanoreactors sticking to the outside of the cells. The cell membrane and the DNA of the HeLa cell were additionally stained with flourophores outside of the excitation and emission wavelength of RB-BSA. This staining of the membrane also helped to localize the cytosol of the cell and therefore get an impression of where the nanoreactors were localized after uptake. The stained DNA shows

indirectly the nucleus of the cell. As transport across the nucleus membrane is highly regulated, nanoreactors were not expected to enter the nucleus as, being around 200 nm in diameter, they are too large to enter.

Confocal laser scanning microscope (CLSM) images only show a cross section layer of the cells containing uptaken dye (nanoreactor). The fluorescent signal of the photosensitizer was therefore expected to be enclosed within the boundary signal of the cell membrane, but not overlapping with the DNA (nucleus) signal. This could be clearly seen in figure 15, where overlying images of all three channels (nucleus, cell membrane and nanoreactors) are separated in space. Therefore, results were compatible with uptake into the cytosol. Similar systems have already been shown to be taken up by cells and be active within the cell [71].

Because with CLSM only qualitative cellular uptake could be seen, flow cytometry measurements were conducted to get a more quantitative readout. A flow cytometer has a flow cell, where HeLa cells can pass through individually and different light scattering and fluorescence data of the cells can be collected. A forward scattering detector (FSC) is able to assess the cell size, while a sideward scattering unit (SSC) gives details about the complexity of a cell, including information on nanoparticle uptake.

Forward scattering helps to detect cells and ignores other particles flowing through the detector. Therefore if a nanoreactor outside a cell would pass the detector individually it could be excluded from the measurement. The SSC in our case detected if cell membranes were still intact. A high signal of sideward scattering indicated that the cells were undergoing apoptosis. With the help of this signal we were able to assess if the cells measured were healthy and exclude the unhealthy cells from the fluorescent measurement. Only a few cells (less than 5%) had to be excluded from the measurements, indicating a high level of viability, as already evaluated with the MTS assay.

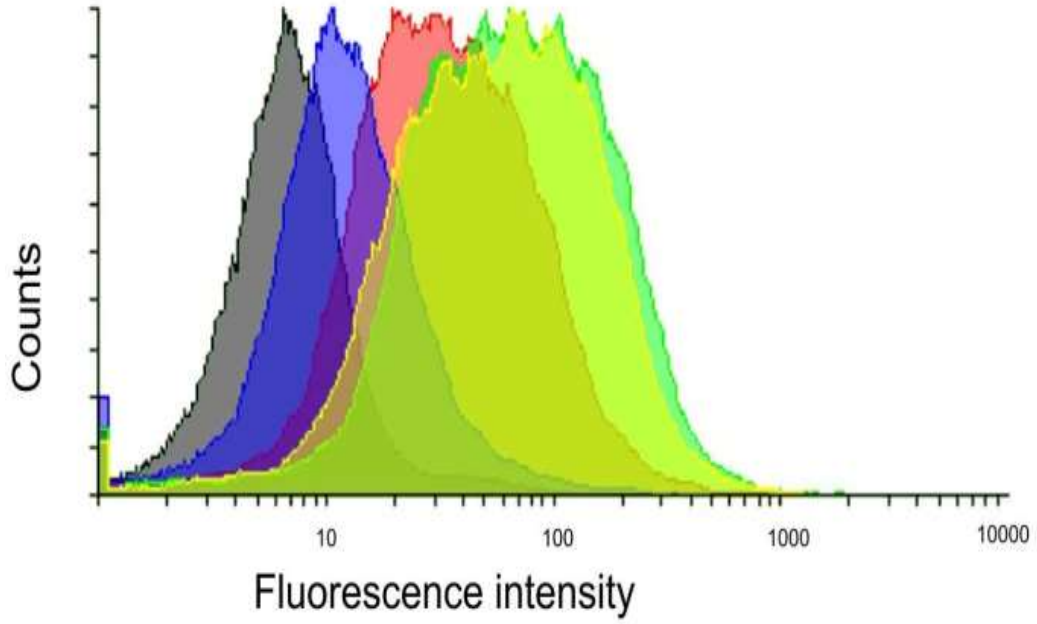


***Figure 13*** *Flow cytometry: cells incubated with A1-200 (green), A3- (yellow), B2- (blue) and B3- (red) nanoreactors and control cells (black). These nanoreactors were tested as they had the best encapsulation efficiency and therefore could bring a higher density of RB-BSA inside cells. The shift towards higher fluorescent intensity indicates a higher fluorescent signal detected in the cells. Therefore A1-200 and A3 nanoreactors were the most efficient vectors for entering HeLa cells.*

The fluorescent signal of RB-BSA was measured simultaneously with the sideward scattering signals giving a quantitative amount of nanoreactors taken up into healthy cells. As control measurements, cells not pre-treated with nanoreactors were measured and taken as a reference for the fluorescent signal shift in the as ahistogram and parameter for optimal uptake (see figure 13). The fluorescent signal of 20'000 viable cell was measured to get good statistics of cellular uptake.

The uptake behavior of the different measured nanoreactors can be seen in figure 13, where the counts were normalized and in which a clear difference in the fluorescence intensity can be seen, indicating an internalization of the nanoreactors into the cells. The PNVP-PDMS-PNVP nanoreactors showed lower uptake that the PMOXA-PDMS-PMOXA based nanoreactors. The uptake behavior was only little different in the case of A1- and A3-nanoreactors. As A1

nanoreactor had less RB-BSA per nanoreactor the efficiency in nanoreactors uptake was probably better with the A1 nanoreactors.

As the uptake can also be size dependent[78-80], different sized nanoreactors based on the A1 polymer were prepared to explore wheter the size of the nanoreactor could help improve the cellular uptake. Therefore A1-200 nanoreactors where further extruded through a 0.1 µm pore size membrane and a part of this solution also through a 0.05 µm pore size membrane. The characteristic of these nanoreactors can be seen in table 2.

Measuring the fluorescence intensity by flow cytometry with cells incubated with the different extruded PMOXA-PDMS-PMOXA based nanoreactors (A1 polymer), no significant difference in the fluorescent signal (uptake of nanoreactor) could be seen. This suggests that the size in the range of 50 nm to 200 nm did not influence uptake.

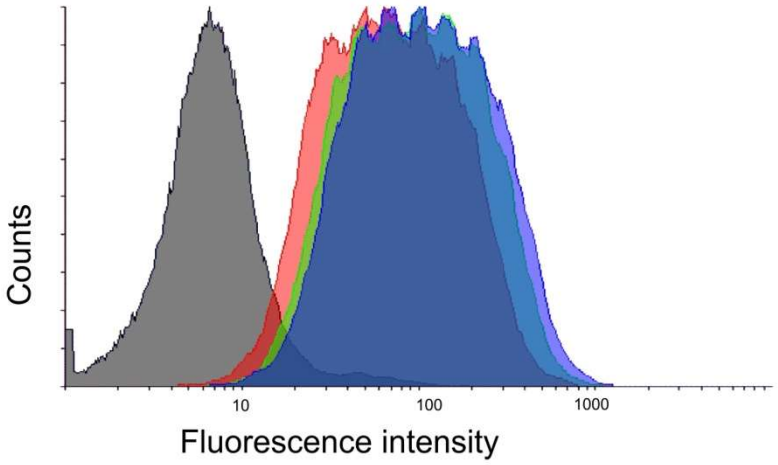


***Figure 14*** *Flow cytometry was used to determine the fluorescence content of cells treated with A1-200(blue), B1-100 (green) and A1-50 (red) nanoreactors loaded with RB-BSA and (black) control cells.*

## 3.12. Stability studies of nanoreactors

Both CLSM experiments and flow cytometry measurements showed that RB-BSA was successfully internalized in HeLa cells with the help of nanoreactors. To prove the integrity of the nanoreactor

system inside cells after uptake, doxorubicin (DOX) was encapsulated in nanoreactors as a control instead of RB-BSA. DOX is used as chemotherapeutic drug[81,82] and intercalates with DNA when freely taken up by cells[82]. Therefore an overlay of the DNA staining signal with the fluorescent signal of DOX would be expected in the case of rupturing nanoreactors inside the cells. In contrast, if the nanoreactor were taken up as a whole and did not degrade after uptake, the fluorescent signal should be exclusively detected, outside of the nucleus and, as-with RB-BSA in the cytosol of the cells. Additionally DOX is a toxic substance, which would lead to cell death, which would also be detected by CLSM, as cells would not be able to stretch anymore.

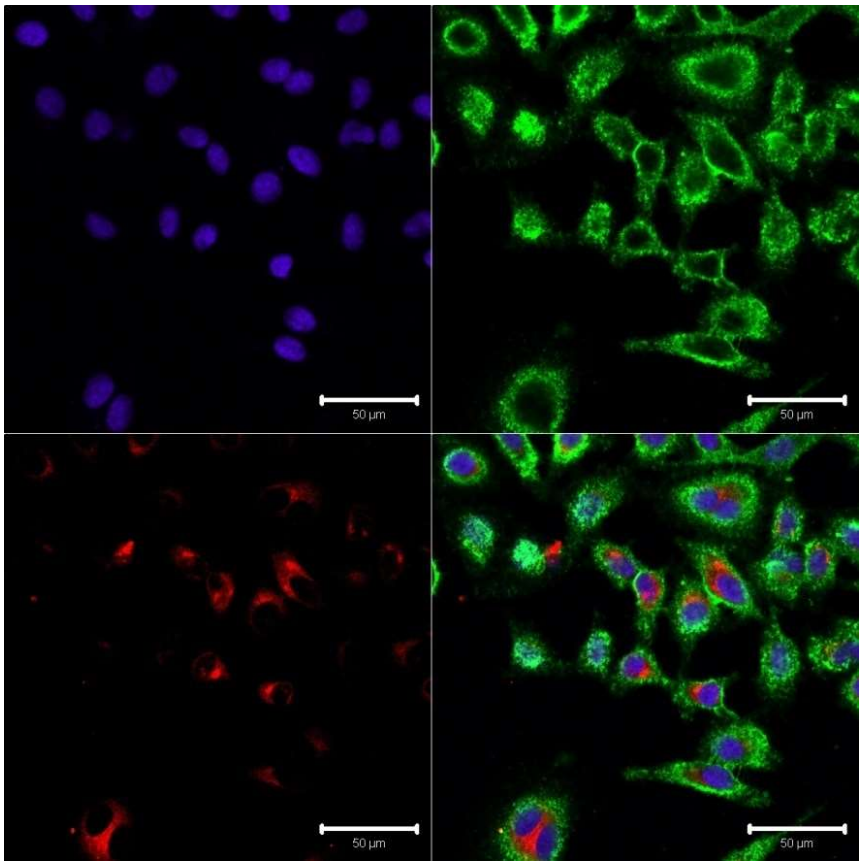


***Figure 15*** *HeLa cells incubated in the presence of doxorubicin loaded nanoreactors. The upper left image shows the fluorescent channel of the DNA staining dye (Hoechst 33342 10 µg ml-1). In the upper right corner the membrane staining is visible, as the borderline of the HeLa cells (Cell Mask Deep Red 5 µg ml-1) Lower left micrograph is showing the fluorescent doxorubicin signal, while the lower right images is the merge of all three individually scanned images. These images show that doxorubicin (encapsulated in the nanoreactors) appeared within the plasma membrane of the cell and not in the nucleus. This finding emphasizes that the nanoreactors can enter the cell, without leaking their doxorubicin content.*

Nanoreactors containing DOX were incubated with HeLa cells and after 24 h prepared for CLSM measurements. The fluorescent signal from DOX was detectable inside the cell, but was not found to overlay with the fluorescent signal of the DNA staining. This indicates that the fluorescent DOX loaded nanoreactors were taken up by HeLa cells, but that DOX was nto further transported into the nucleus. That DOX remained in the cytosol indicates that the nanoreactor system was still stable and no leakage of the encapsulated molecules happened during cellular uptake. This observation is in good agreement with other studies, showing that PMOXA-PDMS-PMOXA based nanoreactors can keep their architecture inside the cell for more than 48 h [71]. This long stability *in vitro* can also promote nanoreactor accumulation in tumor tissues after administration.

The stability of the nanoreactors in presence of light was evaluated by light scattering (LS) and TEM micrographs of A1-200 nanoreactors. LS data show that the size of nanoreactors did not change after illumination (table 3). The ratio between $R_g$ and $R_h$ was around 1 indicating that these measured self-assembled structures were spherical and had an empty core. TEM micrographs showed typical collapsed structures of round objects (see figure 17) – as with nanoreactors left untreated with light - indicating that the morphology does not change upon illumination. In case of loaded RB-BSA nanoreactors, we expected a different reaction as along with the illumination the generation of ROS would start. Still, LS and TEM data indicated that the size and morphology of the nanoreactors was not changed during the production of ROS. The combined stability test of *in vitro* ROS production was not assessed, but it was assumed that the nanoreactors are also stable under irradiation *in vitro*.

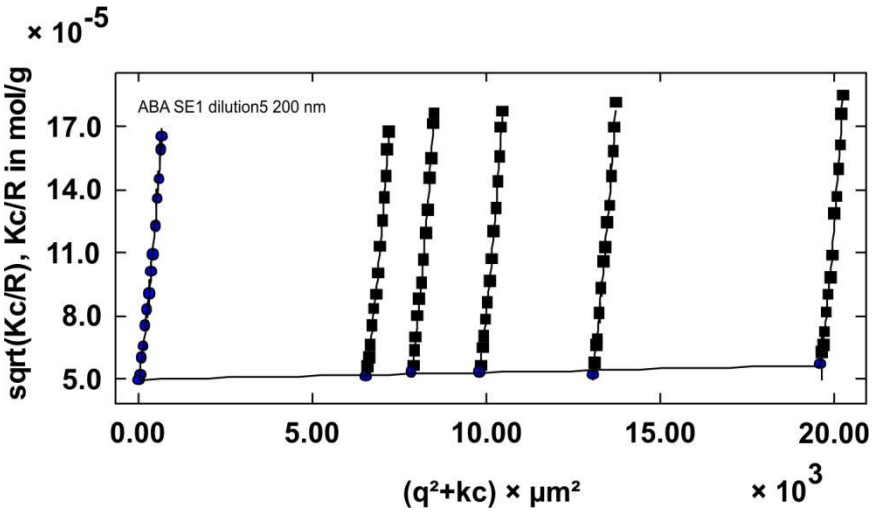


***Figure 16*** *Berry-Plot of A1-200 nanoreactors after illumination.*

***Table 3*** *static and dynamic light scattering data for A1-200 nanoreactors with illumination.*

| | $R_g$ | $R_h$ | $R_g/R_h$ | $M_w$ g mol$^{-1}$ | $A_2$ mol dm$^3$ g$^{-2}$ |
|---|---|---|---|---|---|
| A1-200 | 101 ± 4 nm | 106 ± 2 nm | 0.95 | 1.826x10$^9$ | 3.665x10$^{-10}$ |

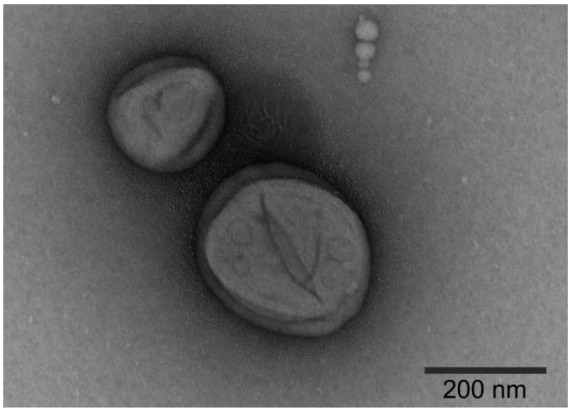


***Figure 17*** *TEM micrograph of nanoreactors after illumination with 90 J/cm2*

## 3.13. In vitro ROS production

After proving that the nanoreactors were taken up as a whole by HeLa cells their functionality inside cells was tested. First, light induced toxicity of nanoreactors was assessed after cellular uptake of the nanoreactors. HeLa cells were incubated with 100 µg/mL A1-200, A1-100 and A1-50 nanoreactor for 24 h and washed with PBS, as it had beed done for MTS viability measurements, CLSM and flow cytometry. After adding fresh media, the cells were illuminated in 96-well plates from the bottom for 0-30 min with an artificial daylight lamp with an intensity of

90 J/cm$^2$. This light intensity is in the normal range in medical use of PDT [83,84], but can also be increased if needed. The use of a specific lamp in the optimal range for ROS production of RB-BSA (530-560 nm) would be beneficial for a medical application.

The viability readout was determined by using MTS assay. Controls with illuminated cells with no nanoreactors, did not show a reduced viability of the cells after illumination, whereas the cell pre-treated with A1 based nanoreactors showed a reduced viability after 30 min. The viability seemed to be decreas linearly with time and reached after 30 min approximately a viability of 50 – 60 % compared to the control cells. The larger nanoreactors A1-200 had a better performance in inducing toxicity than the smaller A1-100 and A1-50 nanoreactors. The induced toxicity was explained by ROS production inside the cell, which was activated by the external light. As only in the presence of light the nanoreactors induce increase in toxicity, we could control the degree of toxicity with the light dose as well by controlling the illumination time.

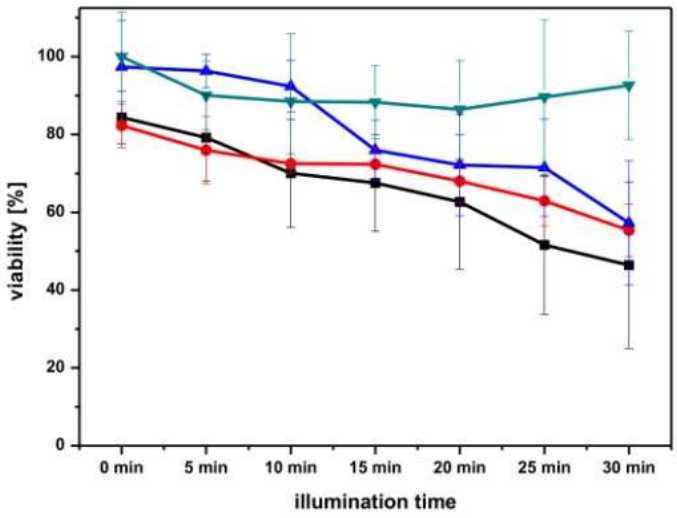


***Figure 18*** *MTS assay of HeLa cells incubated with A1 based nanoreactors of different size illuminated for different periods of time. ▼(green) control cells without nanoreactors,▲ (blue) A1-50-based nanoreactors, ● (red) A1-100 – based nanoreactors, ■ (black) A1-200-based nanoreactors. The viability of the control cells did not change upon illumination, whereas within 30 minutes of illumination up to 50 % of the viable cells died in case of A1-200 nanoreactors.*

To investigate the level of ROS which is produced in cells an experimental setup was established using a non-paramagnetic compound, which is activated only inside cells by esterases. In the presence of esterases the non-paramagnetic compound is transformed into a radical scavenger molecule. The scavenger molecule can then be transformed further in the presence of free radicals into a paramagnetic compound which can be detected by ESR.

1-Acetoxy-3-carbamoyl-2,2,5,5-tetramethylpyrrolidine (ACP) is cell permeable and has an ester bond, which can be cleaved by esterases- only after uptake by cells. The deprotection of ACP leads to a cyclic hydroxylamine, which turns to a nitroxide radical in presence of ROS. To measure the intracellular level qualitatively, control cells were incubated with ACP and the nitroxide level was determined by ESR. A characteristic signal of a nitroxide radical ($a_N$ = 16.1 G) was detected. This weak signal was assigned to the naturally occurring ROS undergoing a reaction with ACP. A higher typical nitroxide radical signal was detected for HeLa cells treated with nanoreactors without illumination. The higher signal could be explained by the fact that the cells are under stress due to the uptake of the nanoreactors. The increase of the intracellular ROS level had no significant influence on the cell viability as already shown (figure 18), and therefore the level of ROS produced by the presence of nanoreactors in the absence of light was not sufficient to induce cell death. Under illumination conditions the intracellular ROS level increased if cells previously had taken up nanoreactors. As the spin count reflecting the amount of nitroxide radical formed increased from 2.65 * $10^8$/mm$^3$ at time point 0 min to 89 * $10^8$/mm$^3$ after 10 min and 105 * $10^8$/mm$^3$ after 25 min irradiation with visible light, we interpretet that this significant increase was the trigger for the increased toxicity observed after illumination.

Despite the increase in ROS levels in the presence of nanoreactors, only the combination of light, oxygen and the encapsulated photosensitizer was able to induce any significant cell death.

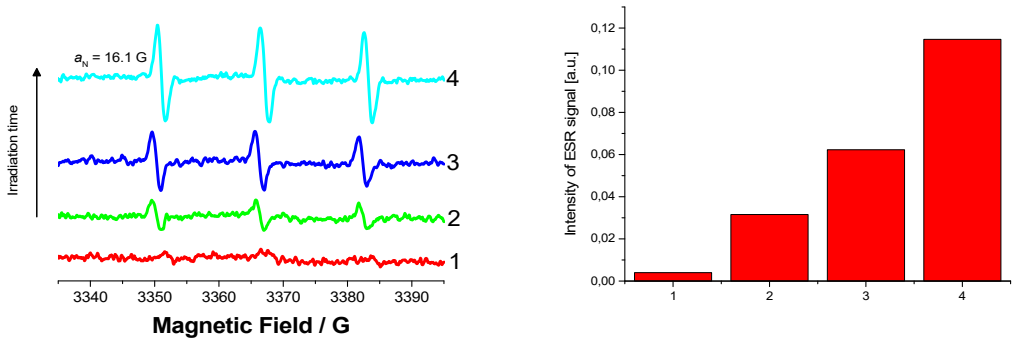


***Figure 19*** *Development of the ESR signal (left) and the integrated intensities (right) with time. 1 are control cells with ACP. 2, 3 and 4r are after 0, 10 and 25 minutes illumination with daylight. The increased signal of 0 minutes illumination compared to the control cells may reflect cells stress due to the uptake of the nanoreactors, but the ROS level is not yet toxic taking other measurements into account.*

## 3.14. Laser light induced ROS production

Laser light was used to localize RB-BSA within the cell and to stimulate the photodynamic activity of RB-BSA. This laser light of 543 nm was only a bit shifted from the optimal excitation wavelength of RB-BSA (560 nm). By using a laser light instead of artificial daylight, the light energy can be more focused and less energy gets lost due to absorbance of others biomolecules in the cell. Additionally, with this laser light the nanoreactors can be precisely stimulated within the cells and locally closed nanoreactors (within a few µm) are not stimulated. This experiment was designed to exploit the unique property of photodynamic therapy, externally activating a nanoreactor taken up by HeLa cells.

Cells pre-incubated with RB-BSA loaded nanoreactor were illuminated for up to 30 minutes with a laser intensity of 23.7 J $cm^{-2}$. The PDT light intensity normally used for treatment in clinical settings is between 30 and 135 J $cm^{-2}$, which is a bit higher than the dose we used in our experiment. After only few minutes of treatment with 543 nm laser light, cells started to form blebs on their membrane. Such blebs are known to be triggered by PDT[85]. These blebs are part of the apoptosis process of the cell and therefore an indicator that cell is dying. Similar phenomena were reported after 24 h after PDT treatment, but we observed blebs formation already after only 5 minutes. The bleb formation could be amplified by a longer illumination time.

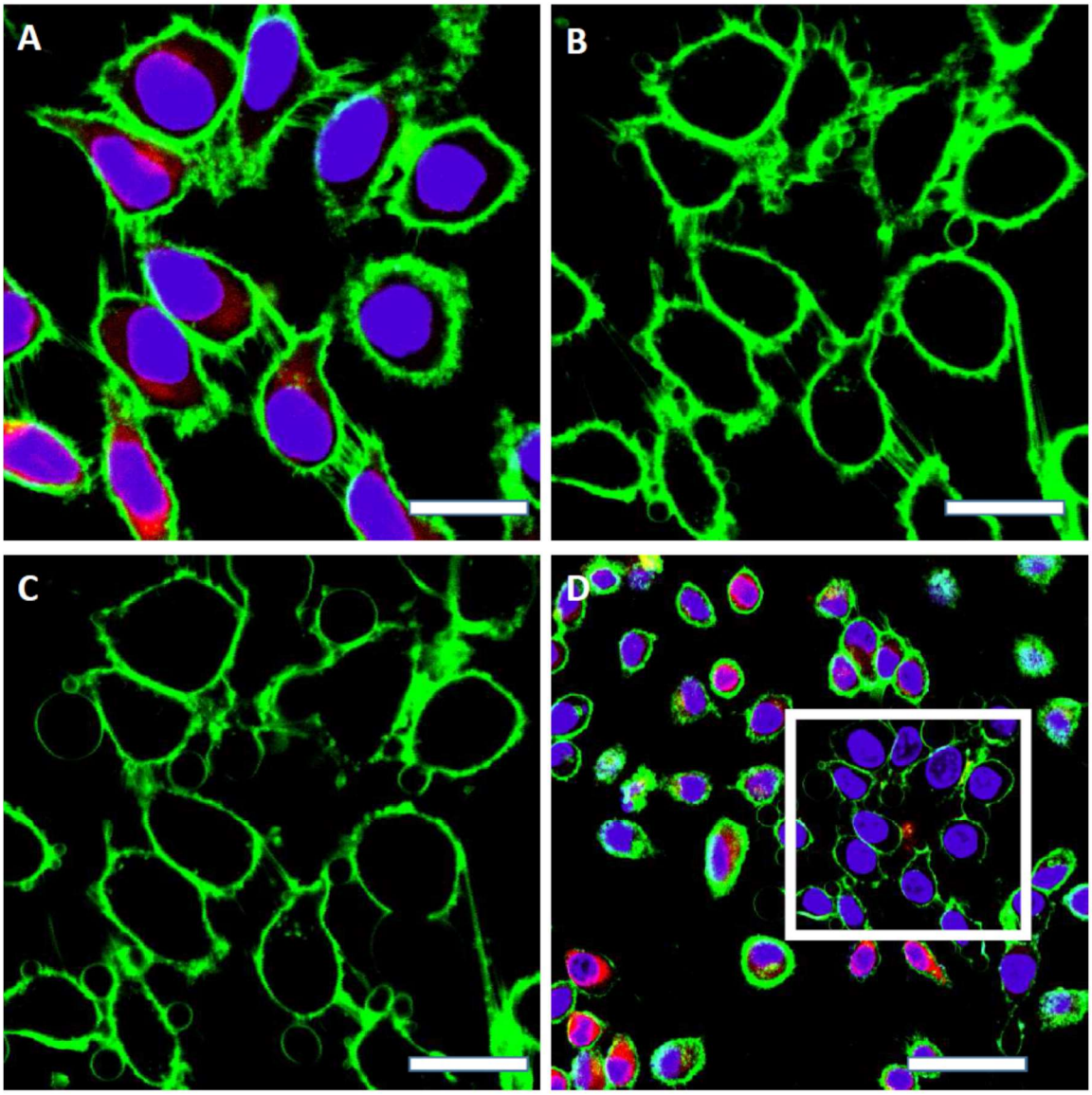


***Figure 20*** *CLSM images of HeLa cells treated with RB-BAS loaded nanoreactors, where the membrane (green, stained with Cell Mask Deep Red 5 µg ml-1 for 5 min) and the DNA (violet, stained with Hoechst 33342 10 µg ml-1 for 10min) were fluorescently labelled. (A) HeLa cells after 24 h incubation in presence of nanoreactors, where the RB-BSA showed a fluorescent signal, which is represented in red color. The cells were nicely attached on the surface and were only minimally exposed to 543 nm light due to image recording reasons. In images (B) only the green fluorescent channel was recorded, while previously the cells had beed illuminated for 4 minutes with 543 nm laser light. The micrograph was taken 6 min after the first exposure to 543 nm laser light. After a total 5 minutes exposure to 543 nm light and 30 minutes after the first light stimuli the cells had created large blebs (C). After zoom out (D) in the treatment area (with square) the cells showed the typical blebs, while outside the illumination area, the cells were not damaged. Scale bar 20 µm (A, B and C) and 50 µm (D)*

When cells exposed to loaded nanoreactors were illuminated with laser light, abundant bleb formation was observed. In control experiments, cells without nanoreactors were illuminated for 30 min and no cell damages were observed. If nanoreactors treated cells were stimulated with

405 nm or 633 nm laser light, they also kept their shape and integrity. This control experiment further supports the selectivity of PDT treatment. By controlling two out of three components (oxygen, light and photosensitizer), local therapy is made possible. Cells neighboring those treated by photodynamic therapy using laser light showed no damage. This observation indicates that the precision of PDT *in vitro* is within a few µm and provides further support that the nanoreactors system is working in a Trojan horse manner, by activing "on demand".

For comparison, HeLa cells with exposed to A1 based nanoreactors only illuminated with daylight were scanned by CLSM. Using the MTS assay it was shown, that cell toxicity could be induced within 25 minutes. CLMS micrographs supported the toxic effect, although less markedly than using laser light (see figure 21). Blebs were also localized, although it is possible that some of the blebs were removed when preparing the cells for these CLSM measurements. Importantly, some blebs were still visible. Moreover, no toxixity difference due to the different sized nanoreactors was observed.

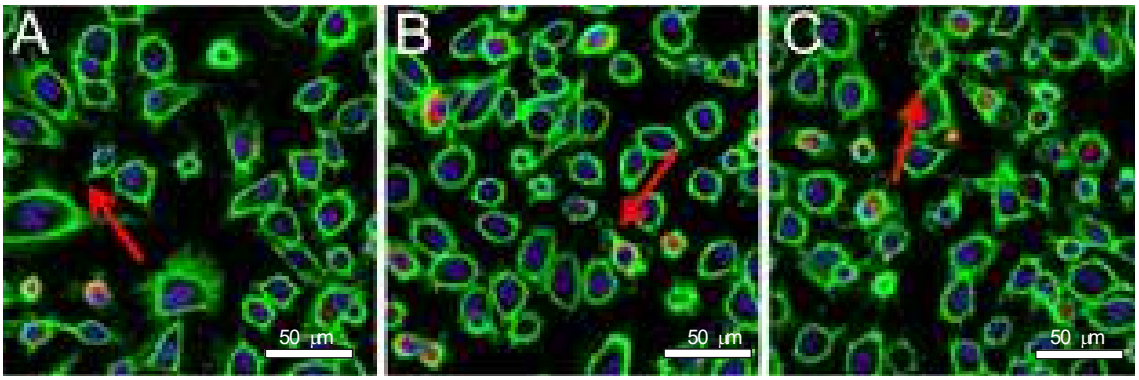


***Figure 21*** *CLSM micrograph of HeLa cells incubated with A1-50 (A) A1-100 (B) and A1-200 (C) nanoreactors and after illumination with 25 minutes daylight (75 J cm-2). The red arrows indicating to bleb formation due to photodynamic activity of the nanoreactors.*

## 3.15. Conclusion

We succeeded in encapsulating a photodynamic active molecule in polymersomes to create a nanoreactor as source of intracellular ROS on demand. We optimized the encapsulation of RB-BSA in different PMOX-PDMS-PMOXA and PNVP-PDMS-PNVP polymersomes to obtain a high loading efficiency. By conjugating RB, which is a highly active photosensitizer, to BSA we increased

the solubility and additionally avoided interaction of RB with the polymer membrane. Therefore we ensured that no RB was attached to the polymersome surface, which could lead to an immune response. The conjugation of RB to BSA lowered the photodynamic efficiency marginally, but the obtained therapeutic results *in vitro* remain promising compared to other photoactive molecules.

The encapsulation inside the nanoreactors had no influence on the photoactivity of RB-BSA and did not present a barrier for the radicals generated *in situ*. The produced ROS could cross the polymeric membrane, while RB-BSA stayed entrapped in the aqueous core. The entrapment of RB-BSA inside the aqueous core of the polymersomes has various advantages: i.) protects RB-BSA from degradation factors ii.) increases the amount of photosensitizer that can be brought into cells at once and iii.) decreases possible side effects occurring from RB toxicity.

The encapsulation efficiency likely depend on the ability to form polymersomes in solution. Therefore the best polymersomes regarding encapsulation efficiency were taken and compared *in vitro*. The sizes of these polymersome were in the range of 200 nm in diameter, which is optimal to fulfil conditions for enhanced permeability and retention effect. All of the nanoreactors were taken up by HeLa cells, while not showing any toxic effect under dark conditions.

The stability of these nanoreactors in cells was also explored and no release of doxorubicin was observed within 24 after uptake of the nanoreactors. Therefore these nanoreactors did not release their content but stayed intact as a Trojan horse inside the cell waiting to be activated by an external stimulus. If irradiated with the proper wavelength, these Trojan became rapidly activated and produced ROS as long as illuminated. By measuring the intracellular ROS level, we found that we could increase the intracellular ROS level by a factor of 40x within 25 minutes under PDT illumination conditions. Along with the increasing ROS content a reduced viability was observed with MTS assays. Additionally we found that cells around the illuminated area were not affected by apoptotic bleb formation, indicating that only the combination of light Trojan horse

and oxygen was effective. Conversely – under dark conditions – cells survived treatment even in presence of these cellular Trojan horses.

The use of light as trigger for ROS production leads to a system that which can be turned on and off externally, providing an intracellular source of ROS “on demand”. The efficiency of such a system, as shown on planar cell culture – as described here - might not be easy to extrapolate to a tissue, although the problem of delivering enough light to the Trojan horses for efficient activity can be solved by exchanging the photosensitizer. For a deeper penetration of light into tissue, light with lower energy has to be used. The advantage of this Trojan horse system is that the photosensitizer can be exchanged and optimized for application. The shell of the Trojan horse – the polymersome – is less exchangeable, as other systems may not be permeable to ROS or induce some toxic effects.

# 4. Enzymatic activity measurements in crowded nanoreactors

## 4.1. Enzyme kinetics

A nanoreactor is depending on an active molecule inside. Besides a photoactive dye, also different enzymes can be encapsulated and their activity in a crowded like environment can be determined. The activity of encapsulated, and free enzyme can be determined spectrophotometrically by following the concentration of produced products. Enzymes and their selective reaction are essential for running the metabolism in living organisms. Enzymes are in most cases built out of amino acid connected with each other's forming a 3D-structure. Some enzymes use cofactors such as ions to assist the catalysis.

A simple enzyme reaction equation is

$$E + S \rightleftharpoons ES \rightarrow E + P$$

Where E is the Enzyme, S the substrate ES the Enzyme substrate complex and P the product of the reaction. This is a simplified equation assuming no back reaction after formation of the reaction product[86]. The kinetics of such a reaction can be described in a general form as:

$$v = \frac{k_{cat}\,[E_0][S]}{K_m + [S]} = \frac{V_{max}[S]}{K_m + [S]}$$

Where v is the reaction rate, $k_{cat}$ the catalytic number, $[E_0]$ the enzyme concentration, [S] the substrate concentration, $K_m$ the Michaelis-Menten constant and $V_{max}$ the limiting rate. In this equation the two fundamental parameter describing enzyme kinetics are present: $k_{cat}$, which describe the catalytic cycles an enzymes undergoes in a certain time and $K_m$ a parameter for the affinity of the substrate to the enzyme[86].

If the initial enzyme concentration $[E_0]$ is unknown $K_m$ still can be determined using a double-reciprocal plot (Linewaever-Bruk plot), where the reciprocal of the initial velocity of an enzyme reaction is plotted against the invers initial substrate concentration, leading to a straight line. The interaction of the resulting line with the x-axis is equal to $-1/K_m$, whereas the intercept is equal to $1/V_{max}$.

A well-studied and characterized enzyme is horseradish peroxidase (HRP)[87]. The mainly used HRP isoenzyme C is a polypeptide having 308 amino acids and a molecular weight of approximately 44

kDa. It has a heme as cofactor, which is responsible for the catalytic activity, in which also $H_2O_2$ is involved.

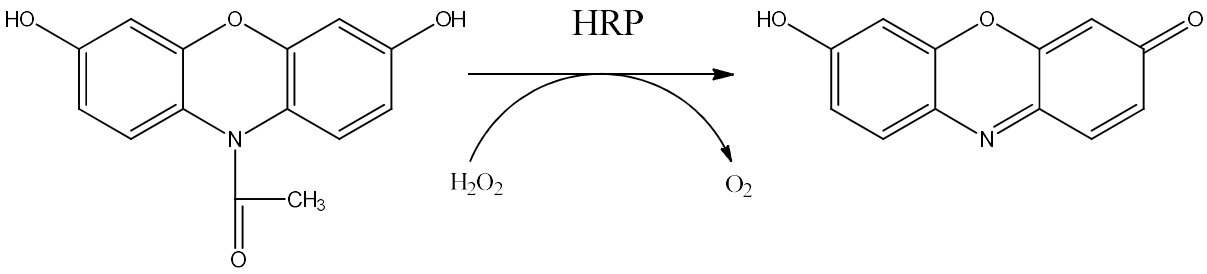


***Figure 22*** *Reaction mechanism of Amplex Red to resorufin in presence of HRP and H2O2.*

In Figure 22 is a model reaction shown catalyzed by HRP. Amplex red is oxidized in the present of $H_2O_2$ and HRP to the fluorescent resorufin with the excitation wavelength of 475 nm at the emission wavelength of 490 nm. Therefore the production of resorufin can be followed and is directly proportional to the product of the reaction. Via this fluorescent measurement the enzymatic kinetic can be observed directly.

## 4.2. Enzymatic reaction in a crowded environment

In a living organism the enzymatic reaction are influenced by crowding agents, which are known to influence the enzyme kinetics[88,89]. The cytosol of a cell is composed of different macromolecules as proteins, nucleic acid or sugars, which have a concentration up to 200-400 g/L[90,91]. Computational simulations already have shown that these macromolecules can influence the enzyme kinetic. Therefore $K_m$ determined in a buffer system without crowding molecules does not represent the real condition an enzyme is working. A systems to understand the enzyme (horseradish peroxidase (HRP)) has been investigated in different crowding milieu as entrapped in an agarose hydrogel[92] or in the presence of dextran[89]. In both cases, the presence of crowding molecules affects the Michaelis-Menten constant, which is a parameter indicating the affinity of the enzyme towards its substrate, has changed. For such enzymatic reaction in a crowded environment mainly highly soluble macromolecules, such as Ficoll, PEG or dextran, are used to mimic a cellular environment [88]. The use of crowding agent for sure is not an exact replacement

for cytosol, but is an approach to get a better understanding of the enzyme kinetic in a more complex system.

## 4.3. OmpF

A nanoreactor is only working if the substrate can enter and the product of the reaction can leave the inside of the nanoreactor. ROS was able to penetrate the PMOXA-PDMS-PMOXA membrane without further help. To guarantee the exchange of substrate for an enzymatic reaction, the membrane has to be designed more permeable.

Nature is using membrane proteins to allow the exchange of molecules across a membrane. It was already shown that is possible to reconstitute different membrane proteins in a polymeric membrane[48]. We used for our purpose OmpF, as it is a channel membrane protein, which allows passive diffusion of molecules. OmpF unselectively let molecules up to 600 Da diffuse through its pore [93,94]. In nature it appears as trimer with single units of about 39 kDa. It is grown in E. coli bacteria and extracted for reconstitution.

## 4.4. Reconstitution of OmpF into polymeric vesicle membranes.

Nanoreactors were prepared with the film rehydration method, while OmpF was added in a detergent containing solution during film rehydration. The hydrophobic character of OmpF matches with the hydrophobic environment of PDMS block in the polymeric membrane, which offers a similar condition as in a lipid bilayer. A successful reconstitution of membrane protein in a polymer membrane depends on two parameters, the thickness and the hydrophobic nature of the polymeric membrane[95]. OmpF insertion in the polymersome membrane increases the permeability of the PMOXA-PDMS-PMOXA membrane. Without a membrane protein the permeability of the membrane is restricted to a few molecules *e.g.* ROS[46,70].

## 4.5. Nanoreactor formation

A crucial step in the nanoreactors formation is the rehydration of the polymer film. During this time the membrane protein gets reconstituted in the polymeric film and the active molecule will

be encapsulated. As the encapsulation is a statistically process not all active molecules will be entrapped in the nanoreactors. Hydrophilic molecules can be better entrapped in the aqueous core of the nanoreactor as hydrophobic ones in the membrane. Hydrophobic molecules can also interfere with the polymeric membrane and can prevent the self-assembly process. Due to high encapsulation degree the presence of the guest molecules influenced the self-assembly behavior. Nevertheless, we succeeded to preserve the self-assembly process in presence of up to 30 mg/ml Ficoll or PEG 3000 in PMOX-PDMS-PMOXA nanoreactors. Beside PEG and Ficoll, also BSA was needed to be encapsulated in higher –amounts for the Trojan horse project, but at a limit of 20 mg/ml BSA –RB was the maximum that did not influence the self-assembly behavior. Higher concentrations of the crowding agents PEG and Ficoll were not used as the self-assembly process did not occur any longer. This could be either due to the increased viscosity or the interaction between the crowding molecules and the polymers was interfering the self-assembly process. To avoid a large size distribution the crowded nanoreactors were extruded through a 200 nm pore size membrane.

## 4.6. Nanoreactor purification

As during the self-assembly process not all molecules were encapsulated in the aqueous cavity of the nanoreactors, free molecules had to be separated. To achieve this size exclusion chromatography (SEC) was used. Compared to dialysis SEC is a faster process and therefore a loss of enzymatic activity due to time issue of the encapsulated active molecules could be reduced or even avoided.

The column packing material was chosen according to the molecular weight of the encapsulated molecules. For proteins and enzymes Sepharose 2B was the preferred material, whereas for dyes and other small molecules Sephadex G-25 was used. The separation process was followed by UV absorbance measurements and the nanoreactors were separated according to their UV absorbance. In the first fraction the nanoreactors and other polymeric superstructures could be

observed, while in the following peaks the not encapsulated molecules were detected. As optimal volume of the separation gel 20 – 25 ml was used. This volume guaranteed separation of vesicular structures as the nanoreactors from the smaller free crowding agent molecules. Additionally, if 1 ml of freshly prepared nanoreactors solution was applied on the column, it lead to an approximately dilution of 1:2. Therefore the polymer concentration was reduced from starting with 5 mg/ml to about 1.66 mg/ml. This value was taken for following calculation of polymer concentrations.

As mobile phase of the column the same buffer as the rehydration one was used. As the reconstituted OmpF allowed the exchange of ions across the nanoreactor membrane, no special treatment was done to avoid different osmolality inside and outside the nanoreactor. The buffer was chosen according to the need of the enzymatic reaction, to obtain a high and specific signal from the enzymatic conversion of the added substrate.

## 4.7. Nanoreactor characterization

To assess the characteristic parameter of the nanoreactors generated for testing enzyme activity, LS and TEM measurements were performed. Knowing that the nanoreactors have a narrow size distribution the influence of the nanoreactor size on the enzyme kinetic can be minimized.

### 4.7.1. Light scattering

Light scattering studies were performed for all nanoreactors to determine $R_h$ and $R_g$ and ρ factor. Light scattering data were calculated using ALV/Static & Dynamic FIT and PLOT program version 4.31 10/10.

***Table 4*** *Light scattering date of HRP containing nanoreactors and nanoreactors formed in the present of crowding agent*

| | $R_g$ (nm) | $R_h$ (nm) | $M_w$ g mol$^{-1}$ | $A_2$ mol dm$^3$g$^{-2}$ | $R_g/R_h$ |
|---|---|---|---|---|---|

| | | | | | |
|---|---|---|---|---|---|
| ABA empty | 144 | 136 | $1.55 \times 10^{9}$ | $5.35 \times 10^{-10}$ | 1.05 |
| ABA 30 mg Ficoll | 145 | 136 | $1.24 \times 10^{9}$ | $4.98 \times 10^{-10}$ | 1.07 |
| ABA 30 mg PEG | 146 | 141 | $1.52 \times 10^{9}$ | $5.36 \times 10^{-10}$ | 1.04 |

Extrusion reduced the size distribution of the nanoreactors, but the diameters of the nanoreactors were higher than the pore size of the extrusion filters. The nanoreactors possess a certain flexibility, so that their real size is larger than the pore diameter. Still extrusion removed aggregates or to larger vesicles. The size distribution and low polydispersity index also indicates that no aggregation in solution was occurring. Furthermore, it indicates that the nanoreactors as we prepared them, are stable and do not fall apart. Free enzymes or crowding molecules would may also interfere with the light scattering signal and show a peak in the range of few nanometers.

The obtained ρ-value (see table 4) are close to one. As an Rg/Rh value of 1.0 is the value for an ideal hollow sphere [52], the measured objects can be regards as hollow spheres, which is the equivalent of a vesicular structure.

### 4.7.2. Transmission electron microscopy

TEM micrographs were taken to support the light scattering data. The micrographs show spherical, but collapsed structures. This suggests that the vesicles were before hollow and collapsed during the TEM-sample preparation. Compared to light scattering, the nanoreactors have to be pre-treated before pictured by TEM. This explains not only the collapse structures but maybe as well the small differences in sizes.

In the TEM images the nanoreactors do not form aggregates and appear as individual objects. This is caused by the pre dilution before preparing for TEM picture but as well from the repellent function of PMOXA.

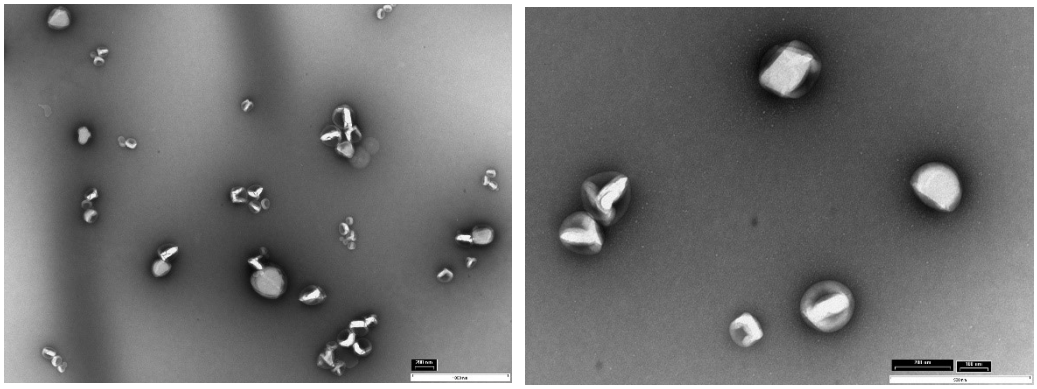

***Figure 23*** *(left) Overview of ABA TH nanoreactor with encapsulated HRP and reconstituted OmpF and (right) zoom view of the collapsed nanoreactor structures. The sizes are in the range of 200 nm which was already proven by light scattering data.*

## 4.8. Encapsulation Efficiency

An important factor for the characterization of nanoreactors is their content of active substance and the crowding agent. The crowding concentration within the nanoreactor will have a direct effect of the kinetic measurements, as the presence of crowding molecules is able to influence the enzymatic kinetic.

Due to the nature of molecules encapsulated, different techniques have to be used to obtain the information of about the EE%. The encapsulated molecules range from small one, like PEG 3000 to larger as Ficoll or proteins/enzymes. As they are also encapsulated in different concentrations (2 mg/mL HRP or 30 mg/mL crowding agent), also other detection limits are applicable. As PEG 3000 and Ficoll are not fluorescent or do not absorb UV-Vis different then the nanoreactor's polymer, the change in the viscosity was used to calculate the encapsulation efficiency for PEG 3000 and Ficoll. The encapsulation efficiency of HRP could not be determined directly by a spectroscopic method as the signal was too low to be detected with the used instruments. By

fluorescent labelling of the enzyme the detection limit could be lowered and the signal was better distinguishable from the polymer absorbance. By using FCS the average number of HRP per nanoreactor was evaluated.

### 4.8.1 Crowding agents

The encapsulation efficiency of Ficoll and PEG was measured by ESR. By co-encapsulating a spin probe (5 doxylstearic acid (5 DSA)) together with the crowding agent, PEG and Ficoll respectively, their intra vesicular concentration was determined *in situ* without modifying the crowding agent or destroying the nanoreactors. The ESR spectra of 5 DSA in 0.1 M NaOH, in empty vesicles, in vesicles loaded with PEG and in free PEG solution (with concentration of 60 mg/mL in water) were measured and are shown in Figure 24. As indicated in Figure 24 free 5 DSA in water shows a typical isotropic triplet with no additional broad signal caused by aggregation and an $a_N$ value of 15.8 G similar with the values reported in the literature[96]. In case of 5 DSA encapsulated in empty vesicles the obtained spectrum presents an anisotropic spectral pattern with the parallel and perpendicular hyperfine components well separated, similar with that described in literature for lipid bilayers[97], indicating that the nitroxide probe is immobilized in the vesicles membrane.

In the presence of 60 mg/mL PEG the obtained spectrum shows the typical isotropic triplet, indicating the free rotation of the spin probe. A broader high-field line characteristic for the nitroxide group indicates the increase in the local viscosity, due to the PEG presence, comparing with 5 DSA measured in 0.1 M NaOH. For 5 DSA encapsulated in PEG loaded vesicles a more complex signal was detected containing both anisotropic spectral pattern due to entrapment in the membrane siloxane layer and the typical isotropic signal indicating a higher mobility component as observed in both 0.1 M NaOH or the 60 mg/ml PEG solution. The isotropic component of the ESR signal detected in loaded vesicles was assigned to encapsulated 5 DSA in aqueous compartment of the nanoreactors, and was further employed to determine the rotation correlation time ($\tau_c$), corresponding to PEG solution encapsulated in nanoreactors.

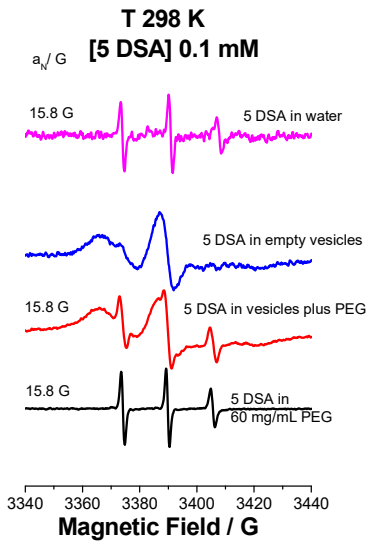


***Figure 24*** *ESR spectra of 5 DSA in PEG aqueous solution, in PEG loaded and empty vesicles and in 0.1 M NaOH*

To determine the average concentration of the crowding agent inside the nanoreactors $\tau_c$ was determined from the experimental ESR spectra of 5 DSA recorded in PEG solutions of increasing concentrations (from 0 mg/mL up to 30 mg/mL) and nanoreactors. $\tau_c$ for the 5 DSA in NaOH was determined as 0.77 nsec similar to literature values[98]. In presence of higher PEG concentration $\tau_c$ increased linearly from 0.91 nsec for 0.5 mg/mL PEG to 2.84 nsec for 30 mg/mL PEG (standard curve) as shown in Figure 2.

$\tau_c$ for the 5 DSA in PEG loaded polymer vesicles (for PEG initial concentration of 30 mg/mL) was determined as 2.27 nsec, corresponding for an intra-vesicular PEG concentration of 21 mg/mL as obtained from the corresponding standard curve depicted in figure 24.

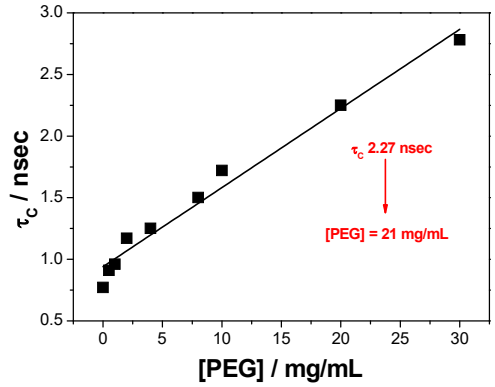


***Figure 25*** *Standard curve for the dependence between PEG concentration and $\tau_c$ of 5 DSA dissolved in increasing PEG concentrations.*

The same experiment was repeated using 20 mg/mL, respectively 10 mg/mL PEG as starting concentration during the film rehydration. The determined $\tau_c$ for encapsulated 5 DSA in the corresponding two types of nanoreactors was determined as 1.79 nsec (for 20 mg/mL PEG), and 1.19 nsec (for 10 mg/mL PEG) corresponding to a final concentration of encapsulated PEG inside nanoreactors of 13.3 mg/mL, respectively 4.1 mg/mL.

A similar behavior was observed in case of 5 DSA in the presence of Ficoll and polymeric vesicles loaded with Ficoll shown in figure 3. For 5 DSA encapsulated in Ficoll loaded vesicles a more complex signal with two different components (one broad signal characteristic for low motion spectra due to the encapsulation in nanoreactors membranes and one isotropic due to the encapsulation inside the nanoreactors) was detected, similar to nanoreactors encapsulating PEG.

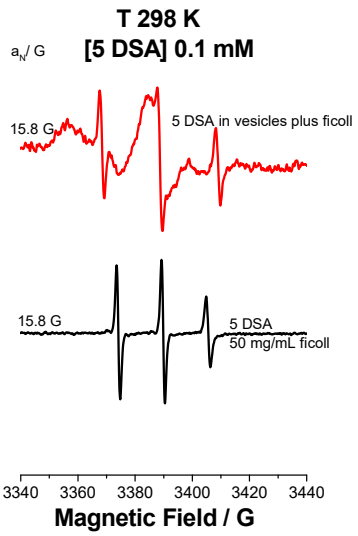


***Figure 26*** *ESR spectra of 5 DSA in Ficoll aqueous solution, and in Ficoll loaded polymeric vesicles.*

A standard curve for 5 DSA in presence of Ficoll was obtained (figure 26), by plotting the $\tau_c$ value of 5 DSA determined in the presence of increasing Ficoll concentrations (from 0.5 to 50 mg/mL Ficoll), against Ficoll concentration. $\tau_c$ values determined for the isotropic component of the ESR signal recorded in nanoreactors were further compared with the standard curve and Ficoll concentration was evaluated. $\tau_c$ for 5 DSA in Ficoll loaded polymer vesicles (when Ficoll starting concentration was 30 mg/mL) was determined as 1.25 nsec, corresponding for a Ficoll concentration of 9.3 mg/mL. In case of loaded nanoreactors with 10, respectively 20 mg/mL starting concentration $\tau_c$ of 5 DSA was determined as 0.93 and 0.97 nsec, corresponding to a local concentration of 2.1 mg/mL and 2.8 mg/mL Ficoll, as shown in Figure 26.

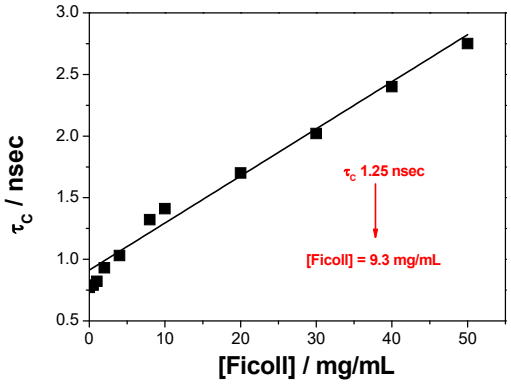


***Figure 27*** *Standard curve for the dependence between Ficoll concentration and $\tau_c$ of 5 DSA dissolved in increasing Ficoll concentrations.*

***Table 5*** *Crowding agent concentration inside the nanoreactor and its corresponding viscosity*

| Starting concentration | Viscosity Ficoll | Viscosity PEG | Ficoll concentration | Viscosity | PEG concentration | Viscosity |
|---|---|---|---|---|---|---|
| 10 mg/ml | 1.018 $m^2s^{-1}$ | 1.022 $m^2s^{-1}$ | 2.2 mg/ml | 0.932 $m^2s^{-1}$ | 4.1 mg/ml | 0.942 $m^2s^{-1}$ |
| 20 mg/ml | 1.129 $m^2s^{-1}$ | 1.158 $m^2s^{-1}$ | 2.8 mg/ml | 0.938 $m^2s^{-1}$ | 13.3 mg/ml | 1.067 $m^2s^{-1}$ |
| 30 mg/ml | 1.240 $m^2s^{-1}$ | 1.293 $m^2s^{-1}$ | 9.3 mg/ml | 1.010 $m^2s^{-1}$ | 21.0 mg/ml | 1.171 $m^2s^{-1}$ |

The encapsulation efficiency (EE%) was determined as 14 – 31 % for Ficoll 41 % and 70 %. For PEG the more than 20 times smaller PEG molecule (3 kDa) was better entrapped as the larger Ficoll dendrimer (70 kDa).

### 4.8.2. Enzyme encapsulation efficiency

HRP was either encapsulated alone or together with the crowding agent. To determine the number of HRP per nanoreactors, HRP was labelled using a labelling kit from life technologies, which labels proteins with Oregon Green®. With an amine-reactive fluorophore a stable covalent bond to a protein can be established. Not reacted fluorophore can be removed with a separation step, while the degree of labelling can be determined spectrophotometrically. The degree of

labelling was 0.7, sufficient enough to determine the encapsulation efficiency for HRP. The diffusion time determined by FCS correlated with the size of the fluorescent labelled molecules or particles, was further used to assess the successful encapsulation of HRP molecules inside nanoreactors. Labelled HRP and encapsulated fluorescent molecules shows larger diffusion times than the free dye[99,100]. The diffusion time measured with FCS increased from 48.8 µs for free Oregon Green to 256 µs for the labelled HRP. Encapsulation of HRP in vesicles with and without crowding agent increased the diffusion time up to 2555 µs for no crowding agent and 2607 µs and 2515 µs for Ficoll respectively PEG loaded nanoreactors. The diffusion times were obtained using a three component fitting, showing that no minor population for free dye or labelled HRP were present after purification.

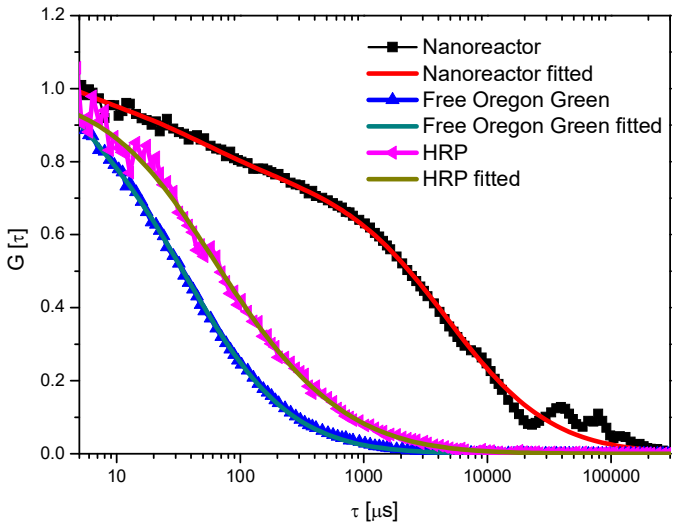


***Figure 28*** *Normalized FCS autocorrelation curves for Nanoreactors loaded with labelled HRP, labelled HRP and free Oregon Green and the corresponding fitting curves.*

***Table 6*** *Data obtained from FCS measurement, where values marked with * are fixed, so that only one component could be determined per measurement.*

| | Count rate [kHz] | CPM [kHz] | C1 [µs] | C1 % | C2 [µs] | C2 % | C3 [µs] | C3 % |
|---|---|---|---|---|---|---|---|---|
| Oregon green | 77 | 13.2 | 48.8 | 100 | | | | |
| Oregon Green in PEG | 77 | 15.2 | 53.2 | 100 | | | | |
| Oregon Green in Ficoll | 76 | 14.7 | 53.8 | 100 | | | | |
| HRP labelled | 22 | 10.7 | *48.8 | 70 | 265 | 30 | | |
| $ABA_{TH}$ encapsulating labelled HRP | 18 | 36.5 | *48.8 | ≈0 | *265 | ≈0 | 2555 | 100 |
| $ABA_{TH}$ Ficoll encapsulating labelled HRP | 26 | 39.0 | *48.8 | ≈0 | *265 | ≈0 | 2607 | 100 |
| $ABA_{TH}$ PEG encapsulating labelled HRP | 8 | 36.5 | *48.8 | ≈0 | *265 | ≈0 | 2512 | 100 |

Comparing the brightness of the particles measured by FCS (free dye and nanoreactors) number of HRP per vesicles was calculated. In all cases (with and without crowding agent) the numbers of HRP per nanoreactors is in average between 3 and 4. FCS measurements and the resulting encapsulation efficiencies show that the crowding agents do not influence the encapsulation efficiency of HRP. Nevertheless, due to the low degree of labelling and the uncontrolled self-assembly processes, there is the theoretical possibility to have none enzyme in a vesicles or to have more the 4 enzymes per vesicles. The amount of HRP per nanoreactor is in good agreement with other similar system and labelled enzymes[101,102].

The encapsulation efficiency of HRP, if compared with the starting concentration, is between 9.7% and 11.2%. This is in the typically range for PMOXA-PDMS-PMOXA based nanoreactors produced by film rehydration[49,51,69,102].

The simplest way to calculate encapsulation efficiency is by comparing the initial concentration with the concentration encapsulated. This was mainly done for encapsulation of RB-BSA, as RB-BSA could not be detected with FCS. A dependence in encapsulation efficiency depending on polymer properties or nanoreactor size could not be observed. At low initial concentration the encapsulation efficiency was around 13 % and lower, depending on the ability to form vesicles.

Encapsulation of macromolecules at a high initial concentration (>10mg/ml) several small trends could be observed. PEG 3000 was better encapsulated in the nanoreactors as the almost ten times bigger Ficoll macromolecule.

It was also observed that the encapsulation efficiency is depending on the starting concentration if ($C_0 \geq 10$ mg/ml). For both Ficoll and PEG 300 the encapsulation efficiency is higher if the concentration used in the rehydration mixture is higher. An explanation for this is, that higher the initial concentration is higher the chance induced by crowding molecule it gets.

## 4.9. Enzymatic activity in the nanoreactors

HRP is one of the best characterized enzymes which have found various application in industry, science and even medical applications [87]. In literature, the reaction with amplex red under similar conditions as we have performed our kinetic measurement, the value of the Michaelis-Menten constant is around 81 µM[103]. To avoid difference coming from experimental details we have performed enzymatic reaction for different situations (crowding and encapsulation) under the same condition (buffer, temperature, $H_2O_2$ concentration and Amplex red concentration). To exclude pipetting errors of small volumes enzymatic reaction were performed in a multi-well plate to perform several kinetic runs in parallel.

In a first trial the kinetic of free HRP in bulk in the absence of crowding molecules was done and a $K_m$ value of around 55 µM , close to the value already reported was obtained. By adding Ficoll or PEG up to concentrations of 30 mg/mL in 10 mg/mL steps we observed that $K_m$ values were influenced by the presence of the crowding agent. In case of Ficoll the $K_m$ value was around 31 µM for all three measured crowding agent concentrations. In the presence of PEG the $K_m$ value decreased even more around 25 µM. This already shows that the crowding agent has a dramatic influence on the kinetic of an enzyme. In our case, the crowding agent had not only induce a decrease of the $K_m$ value, but also a different behavior has already been reported for other enzymes [88,104]. A decrease of the $K_m$ value from 55 µM to 31 µM, 25 µM respectively, means that the enzyme-substrate affinity is almost doubled. Due to the presence of the crowding agent, the substrate has less space in the aqueous phase and the possibility to interact with the active side of HRP can be increased. Additionally the crowding molecules can have a positive effect on the stability of the enzyme or the substrate during the reaction, but experiments in this direction were not performed.

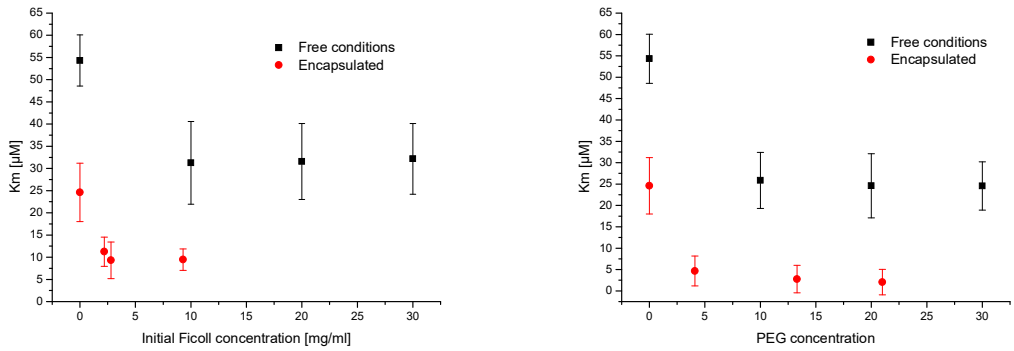


***Figure 29*** *(left) Michaelis-Menten constant of HRP in the present of different Ficoll concentrations (black) and encapsulated with different Ficoll concentrions (red). (right) Michaelis-Menten constant of HRP in the present of different PEG 300 concentrations (black) and encapsulated with different Ficoll concentrions (red).*

## 4.10. Conclusion

A successful combination of biologicals entities and synthetic materials is still a challenge for diagnostic purpose or engeneering devices at the nanometer scale [Baumann_2011]. By reconstitution of the membrane protein in a polymeric membrane and simultaneously encapsulating an enzyme, shows that hybrid material (synthetic-biologic) can have great opportunities to answer scientific questions or to help increasing efficiency and stability of an enzyme. A still not completely solved question is the one of enzymes kinetic in cellular conditions. With the encapsulation of enzymes in nanoreactors we tried to simulate an artificial organelle and additionally tried to mimic a crowded environment with macromolecules to get a better understanding of enzyme kinetics under cellular conditions.

The use of a high density of macromolecules affects the self-assembly process of nanoreactors which shows that there are limitations for the self-assembly process. In the presence of 30 mg/mL macromolecules it is still possible to form self-assembled nanoreactors while reconstituting OmpF and encapsulating HRP, while at higher concentartion the self-assembly process is not occuring anymore in a proper way to obtain nanoreactors.

The concentration of macromolecules inside the nanoreactors is not equal to the macromolecular concentrations of the rehydartion solution. Comparing the concentration inside the nanoreactors with the concentration before the encapsulation, we have seen that smaller macromolecules (3 kDa) have a better efficiency to be entrapped as larger (70 kDa). Using the same starting density (in mg/mL) of the macromolecules the smaller molecules have double the density in the nanoreactors as the larger one. Also the enzymes as a larger macromolecule (44 kDa) showed encapsulation efficiencies around 10% or 3-4 enzymes per nanoreactor.

We showed that the enzyme kinetic is not only affected by the crowding molecules PEG and Ficoll, but as well by the restricted space in the aqueous cavity of the nanoreactor. This system is maybe far of simulating cellular conditions, but represent a smart approach to show the influence of

crowded environment and confined space. The activity of the enzyme can be tuned due to encapsulation and crowding agent, which may in some cases improve enzyme activity. Such a crowded nanoreactor can also be considered as a further step towards an artificial cell or organelle, as the enzyme was compartmentalized but still interacting with the environment through the channel proteins.

# 5. General conclusion and outlook

As it was shown within this thesis the possibility of using polymersomes can have great advantages compared to existing methods. Nevertheless both systems can still be improved and have to be further tested for a real applications. The enzymatic assays have to be repeated with other enzymes or other substrate to see if the system is also working under these conditions. For the Trojan horse a sterile way of producing the polymersome has to be found, so that a next step of *in vivo* studies can be performed.

By synthesizing different block ratio of the polymers there can be found maybe a more optimal polymersome structure for the applications, but this has to be done with try and error, as the Trojan horse experiment have shown, there is no specific trend comparing block ratio and encapsulation efficiency or polymersome formation.

# 6. Materials and Methods

## Materials

Materials were ordered from Sigma Aldrich id not further noticed and used without further treatment.

## Rose Bengal-BSA conjugation[51]

20 mg (300 µM) bovine serum albumin (BSA) was dissolved in 1 ml PBS solution containing 100 µM Rose Bengal (RB). After 1 h at room temperature the solution was applied on a HiTrapDesalting column containing Sephadex™ Superfine (GE Healthcare, UK). The successful conjugation can be followed using UV-Vis spectroscopy recording 550 nm and 560 nm.

## Vesicle formation[51]

The synthesis and characterization of PMOXA-PDMS-PMOXA and PNVP-PDMS-PNVP polymers used for these studies is described elsewhere. For the formation of polymeric vesicle film rehydration method was used. First the polymer was dissolved in pure ethanol. Afterwards 5 mg of dissolved polymer was added to a 25 ml ethanol-cleaned round-bottom flask and ethanol was evaporated at a reduced pressure of 150 mbar in a rotary evaporator (Büchi Rotavap R-124 with vacuum controller B-721, Büchi, Switzerland) at 40°C while rotating at 100 rpm for 30 min to obtain a polymer film on the inner glass surface of the flask. In a final step pressure was reduced to 100 mbar for an additional 5 min.

The encapsulating solution was premixed and the volume was adjusted to 1 ml. The solution was added to the 25 ml round-bottom flask with the polymer film and stirred overnight under atmospheric pressure. The film rehydration was performed at room temperature or at 4°C depending on the stability of the encapsulating molecules. The flask was tilted, so that the whole polymer film was detached from the glass surface.

To obtain uniform size vesicles, the rehydrated solution was extruded with a LipoFast-Basic extruder (Avestin, Canada) through a 0.2 µm Track-Etch membrane (Whatman, UK). If necessary other filter membranes (0.4 µm, 0.1 µm and 0.05 µm) were used. After extrusion the vesicle

solution was applied on a size exclusion chromatography (SEC) column filled with Sepharose 2B connected to an ÄKTA prime (GE Healthcare, UK). The elute was recorded using a UV detector (280 nm) and fractionated according to de appearing peaks.

## Light Scattering[51]

Light scattering experiments were performed using an ALV goniometer (ALV GmbH, Germany) equipped with an ALV He-He laser (JDS Uniphase, wavelength λ = 632.8 nm). The vesicle solutions (1.0, 0.66, 0.5, 0.4, 0.33 mg $ml^{-1}$) were measured in a 10 mm cylindrical quartz cell at angles ranging from 30° to 150° at 293 K. ALV/Static & Dynamic FIT and PLOT program version 4.32 10/10 was used to analyzed the data. Static light scattering data were processed according to the Gunier-model.

## Transmission electron microscopy[51]

10 ml empty polymer vesicle solution and an RB–BSA conjugate loaded polymer vesicle solution were negatively stained with 2% uranyl acetate solution and deposited on a carbon-coated copper grid. The samples were examined with a transmission electron microscope (Philips Morgani 268 D) operated at 80 kV.

## OmpF expression and purification[105]

OmpF was expressed into the host *E. coli* BE strain BL21 (DE) omp8 (F_hsdSB (rb_mB) gal ompT dcm(DE3) DlamB ompF::Tn5 DompA DompC).

OmpF expression and purification was adapted from Nallani *et. al*[106]. An overnight culture was used to inoculate 1L LB medium containing 100 µg/mL ampicillin starting with an OD600 of 0.1 (250 rpm, 37°C). Reaching an OD600 of 0.6, isopropyl-β-D-thiogalactopyranoside (IPTG) was added to a final concentration of 1 mM to induce expression of OmpF. Cells were grown for additional 4 h, following harvesting by centrifugation (10 min, 6000 rpm, 4°C). The cell pellet was resuspended in 10 ml lysis buffer (20 mM Tris-Cl pH 8.0, 2% SDS) per 1g of cell pellet. The resuspended cells were shortly sonicated and passed three times through a high-pressure

homogenizer at 2000 bar. Afterwards the homogenized solution was centrifuged (40 min, 22000 rpm, 4°C) and the obtained pellet was further used

The pellet was resuspended (0.125% octyl-POE in 20 mM phosphate buffer pH 7.4) for a pre-extraction step and incubated for 1 h at 37°C. After an additional centrifugation step (40 mi, 40000 rpm, 4°C) the remaining pellet was further treated with 3% octyl-POE in 20 mM phosphate buffer pH 7.4 for the final OmpF extraction. In a final centrifugation step (40 min, 40000 rpm, 4 °C) the solubilized OmpF was separated from the membranes.

The expression and the purity were verified by SDS-PAGE (12%). The concentrations were determined spectrophotometrically at 260 nm and the sample stored at 4°C till use.

## Cell culturing

Cell culture was started using a stock culture containing 1 million cells in 10 % DMSO. The stock culture was defrosted and diluted with culture medium (DMEM with 10% FCS and 2% Pen/Strep). After centrifugation (10 min at 1000 rpm, approx. 200??) supernatant was removed and fresh culture medium was added. Afterwards, the resuspended cells were incubated in a 75 $cm^2$ flask (BD Falcon, USA) at 37° C and 5% $CO_2$. Cells were split twice per week, removing the culture medium, rinsing with PBS and trypsinizing. Before that, the solution was centrifuged and the supernatant was removed and the cells were resuspended in fresh culture medium. Cell density was determined using Countess® Automated Cell Counter (Invitrogen, USA). For continuing cell culture 1 million cells were incubated in cell culture flask and fresh medium was added up to a volume of 25 ml. For experiments cells were taken and incubated on well plates for at least 24 h before experiments.

## Cell toxicity assay[51]

2 x $10^4$ HeLa cells per well were cultured in 200 µl fresh culture medium for 24 h in a 96-well plate. Afterwards medium was exchanged and the cells were incubated with different concentrations

of nanoreactors (50 – 500 µg/ml) keeping the volume constant. Differences in concentration were adjusted using PBS. After the desired incubation time the culture medium was exchanged and 20 µl of MTS (3-(4,5-dimethylthiazol-2yl)-5-(3-carboxymethoxyphenyl)-2-(4-sulfophenyl-*2H*-tetrazolium) assay solution (Promega, USA) was added. After 1 h incubation with MTS, the absorbance of each well was measured at 490 nm with a microplate reader (SpectraMax M5$^e$, Molecular Devices, USA). Cell viability was calculated assuming cells grown without the presence of nanoreactors and background corrected with culture medium and MTS assay solution as 100% viable.

## Uptake studies (CLSM)[51]

For microscope experiments HeLa cells were cultured at a density of 5 x $10^4$ cells per well in a 8-well Lab-Tek™ (Nalge Nunc International, USA) in 300 µl culture medium for 24 h to allow attachment to the surface. After attachment, the medium was removed and nanoreactor solution in DMEM growth medium without FCS was added. After the desired incubation time cells were stained with the desired dyes.

***Table 7*** *Used dyes for cell staining and its incubation time and used lasers.*

| Dye | Stock concentration | incubation volume | Incubation time | Used laser | Staining compartments |
|---|---|---|---|---|---|
| Hoechst 3342 | 100 µg/ml | 20 µl | 10 min | 405 nm | DNA (nucleus) |
| Cell mask Deep Red | 50 µg/ml | 20 µl | 5 min | 633 nm | Cell membrane |
| Lysotrack Deep Red | 1 µM | 20 µl | 10 min | 633 nm | Acid compartments |

After incubation with dyes, cells were washed three times with PBS and let in 300 µl PBS. Cells were visualized using a confocal laser scanning microscope (Carl Zeiss LSM510, Germany) equipped with a 40x water emulsion lens (Olympus, Japan). The cells micrographs were recorded

in multitrack mode and the intensity of each fluorescent dye was adjusted individually. For control micrographs same setting were used as for sample micrographs. Carl Zeiss software (version 4.2 SP1) was used to record and images processing.

## Uptake studies (Flow cytometry)[69]

1 x $10^5$ HeLa cells were seeded in a 24-well plate and grown for 24 h in culture medium (1 ml). After 24 h medium was exchanged and nanoreactor solution with DMEM growth medium was added. After 24 h incubation in presence polymeric vesicles cells were washed with PBS, trypsinized, centrifuged, resuspended in PBS and put on ice. Flow cytometry was measured with a BD FACSCanto II flow cytometer (BD Bioscience, USA) using FCS and SSC detectors as well as fluorescent channel for RB-BSA. A total amount of 20'000 events for each samples were analyzed. Data treatment was done using Flowing Software 2.5.0 (Turku Center for Biotechnology, Finland).

## In vitro radical measurement[69]

The cell culturing was adapted from Pierzchala. 2 x $10^5$ HeLa cells per well were cultured in Dulbecco's Modified Eagle's Medium (DMEM) containing 10% fetal calf serum (FCS) in a 6-well plate for 24h at 37°C in humidified $CO_2$ incubator. Afterwards the cells were incubated for another 24h in DMEM and the present of the vesicles. The cells were washed twice with PBS and then incubated under dark conditions at room temperature for 90 min with 10 mM 1-Acetoxy-3-carbamoyl-2,2,5,5-tetramethylpyrrolidine (ACP) (Enzo Life Sciences, Switzerland). Afterwards the cell were detached and centrifuged at 1000 rpm for 5 min. The supernatant was removed and the cell were resuspended in 200 µl PBS and transferred into a glass pipette.

The samples containing ACP, cells, cells and ACP, cells and RB-BSA loaded vesicles were measured as prepared, before and after 5-20 min irradiation. The quantitative determination was performed using the SpinCount and internal reference provided by Bruker with the spectrometer.

The DMPO spin adducts were obtained by mixing 0.1 mL of 1 mM DMPO solution in PBS with 0.5 mL Rose Bengal 4 µM RB-BSA or 0.5 mL ABA SE1 polymersomes loaded with RB.

ESR measurements were performed on a Bruker CW ESR Elexsys-500 spectrometer equipped with a variable temperature unit. The spectra were recorded at 298 K with the following parameters: microwave power 2 mW, number of scans up to 20, resolution 2048 points, modulation amplitude 0.5 G. ESR spectra were simulated using the WINSIM 2002 (NIEHS/NIH) simulation package[3]; that allows the determination of the hyperfine couplings line width with an error of 5%.

## Radical detection with ESR

2,2,6,6-Tetramethyl-4-piperidinol (TMP–OH) powder was weighed and a solution with the same amount of RB was added to the powder to obtain a concentration of 200 mM. In the case where RB, RB–BSA, and the vesicle solution did not have the same absorbance at 550 nm and 560 nm, the sample was diluted with PBS until they all had the same RB concentration. The ESR experiments were carried out at room temperature using an ESP300E spectrometer (Bruker BioSpin, Germany) operating at the X-band frequency and equipped with a standard rectangular mode TE102 cavity. Samples were transferred to 0.7mmID and 0.87 mm OD glass capillary tubes (VitroCom, NJ, USA), with sample height _50 mm (_20 ml), and sealed on both sides with Cha.seal (tube sealing compound, Chase Scientific Glass, Rockwood, TN, USA). An assembly of seven tightly packed capillaries was bundled together and inserted into a wide-bore quartz capillary (standard ESR quartz tube with 2.9 mm ID and 4 mm OD, Model 707-SQ-250M, from WilmadGlass Inc., Vineland, NJ, USA). This setup resulted in ca. 140 ml sample volume in the active zone of the TE102 cavity. The samples were illuminated with visible light and measured with the typical instrument settings: microwave frequency 9.77 GHz, microwave power 10.1 mW, sweep width 100 G, modulation frequency 100 kHz, modulation amplitude 0.5 G, receiver gain 2 _ 104, time constant 81.92 ms, conversion time 40.96 ms and total scan time 41.9 s.

## ESR measurements for intravesicular viscosity measurement

ESR measurements were performed on a Bruker CW ESR Elexsys-500 spectrometer equipped with a variable temperature unit. The spectra were recorded 298 K with the following parameters: 100 KHz magnetic field modulation, microwave power 2 mW, conversion time 61.12 ms, number of scans up to 20, resolution 2048 points, modulation amplitude in the range of 0.4 G, sweep width 100 G. The nitrogen hyperfine coupling ($a_N$) was determined directly from the spectra for motional narrowed lineshapes with an error limit of 5%. The microviscosity in proximity of the nitroxide free-radical probe was determined by the means of the correlation time $\tau_c$ related to the rotational reorientation of the probe:

$$\tau_c = 6.5 * e^{-10} * \Delta H_0 * \left\{ \sqrt{\frac{I_0}{I_{+1}}} - 1 \right\}$$

, where $\Delta H_0$ is the linewidth of the 0 transition, $I_0$, $I_{+1}$, $I_{-1}$ are the peak to peak heights of the 0, +1 and -1 transitions.

## ESR Control experiments

In order to determine the dependence of $\tau_c$ of the spin probe of concentration of both PEG and Ficoll, series of solutions containing 0.1 mM 5 DSA in 0.1 M NaOH and PEG in concentrations varying from 0.5 mg/mL to 30 mg/mL or Ficoll ranging from 0.5 mg/mL to 50 mg/mL were measured. $\tau_c$ was determined for each solution and the standard curve obtained by fitting linear all the points describing the dependence of $\tau_c$ to PEG or Ficoll concentration was obtained.

## Fluorescence labelling of HRP

HRP was labeled fluorescently using Oregon Green ® 488 Protein Labeling Kit (O-10241) from life technologies and used according their protocol. The labelling efficiency was calculated according to the given protocol using the specific absorbance of HRP at 403 nm and the absorbance of Oregon Green at 496 nm. The absorbance was measured spectrophotometrical using nanodrop 2000c (ThermoScientific, USA).

## Fluorescence correlation spectroscopy (FCS)

A Zeiss510/Confocor2 laser scanning microscope equipped with an argon laser (488nm) and a 40 x water-immersion objective (C-Apochromat 40X, NA 1.2) with a pinhole adjusted to 70 µm was used in FCS mode to measure solution of Oregon Green, labelled HRP, and vesicles encapsulating labelled HRP separately at room temperature. FCS spectra were recorded over 10 s and measurement was repeated 30 times. For autocorrelation function and fitting LSM510/confocor software package version 4.2 SP1 was used, were structure factor and diffusion times of individually measured free dye and labelled HRP, were fixed for the fitting procedure.

## Encapsulation efficiency calculation [69]

Encapsulation efficiency of the vesicle formation process [EE%] was determined as following:

$$EE[\%] = \frac{concentration\ after\ encapsulation\ and\ purification}{concentration\ before\ encapsulation} \times 100$$

Therefore the absorbance of the to-be encapsulated solution was compared with the nanoreactors after size exclusion. Additionally the volume was corrected, to deal with the dilution occurring during size exclusion chromatography.

The maximum number of RB-BSA conjugates (#RB-BSA$_{per\ vesicle}$), which can be encapsulated per vesicle was calculated using:

$$\#\mathrm{RB-BSA}_{per\ vesicle} = C_0 \times N_A \times {}^{4}/_{3} \times \pi \times R_h^3 \times 1000 \qquad \text{(eq. 2)}$$

where $C_0$ is the concentration of RB-BSA conjugates encapsulated [mol/L], and $R_h$ is the hydrodynamic radius of vesicles [m] obtained from light scattering.

## Kinetic measurement [107]

Amplex ultra red (AR) (Invitrogen, US) was dissolved in DMSO as 10 mM stock solution. A 96-well microplate (BD Bioscience, US) was used to perform 8 parallel kinetics measurements for each substrate concentration. The wells were filled up to 200 ul with PBS containing Nanoreactors/HRP, 2, 4, 8 or 12 µM AR and an excess of $H_2O_2$ (20 µM). The kinetic was recorded at 25 °C with a SpectraMax M5e (MolecularDevices, US) measuring each 20 second after shacking

the fluorescence signal of AR (570nm/595nm). For the calculation of the Michaelis-Menten-constant ($K_m$) the initial rate was determined by linear regression analysis of the slope ($R^2$>0.99). Further calculations were performed by using Origin and MS Excel software packages.

## Abbraviations

| | |
|---|---|
| ACP | 1-Acetoxy-3-carbamoyl-2,2,5,5-tetramethylpyrrolidine |
| AFM | Atomic force microscope |
| AqpZ | Aquaporin Z |
| BSA | Bovine serum albumin |
| CLSM | confocal laser scanning microscope |
| CPM | counts per molecule |
| Da | dalton |
| DMPO | 5,5-dimethyl-1-pyrroline *N*-oxide |
| DNA | Deoxyribonucleic acid |
| DOX | doxorubicin |
| EE% | encapsulation efficiency |
| EPR | enhanced permeability and retention effect |
| ESR | Electron spin resonance |
| EtOH | Ethanol |
| FCS | fluorescence correlation spectroscopy |
| FhuA | ferric hydroxamate uptake protein component A |
| FSC | forward scattering |
| h | hour |
| HRP | Horseradish peroxidase |
| K | Kelvin |
| $k_{cat}$ | catalytic number |
| $K_m$ | Michaelis-Menten constant |
| MTS | 3-(4,5-dimethylthiazol-2-yl)-5-(3-carboxymethoxyphenyl)-2-(4-sulfophenyl)-2H-tetrazolium |
| OmpF | Outer membrane protein F |
| PAA | poly(acrylic acid) |

| | |
|---|---|
| PAGE | polyacrylamide gel electrophoresis |
| PB | Poly(butadien) |
| PBS | phosphate buffered saline |
| PCV | polyvinyl chloride |
| PDMA | poly(2-(diisopropylamino)ethyl methacrylate) |
| PDMS | poly(dimethylsiloxane) |
| PDT | photodynamic therapy |
| PEG | polyethylene glycol |
| PEO | Poly(ethylene oxide) |
| PET | polyethylene terephthalate |
| PLA | poly(lactide) |
| PLC | poly(ε-caprolactone) |
| PLGA | poly(lactic-co-glycolic acid) |
| PMPC | poly(2-methacryloyloxyethyl phosphorylcholine) |
| PMOXA | poly(2-methyl-2oxazoline) |
| PNVP | poly(N-vinylpyrrolidone) |
| PS | poly(styrene) |
| RB | Rose Bengal |
| $R_g$ | Radius of gyration |
| $R_h$ | Radius of hydration |
| ROS | reactive oxygen species |
| SDS | sodium dodecyl sulfate |
| SEC | size exclusion chromatography |
| SSC | sideward scattering |
| TEM | transmission electron microscopy |
| TEMPOL | 4-hydroxy-2,2,6,6-teramethyl piperidin-1-hydroxyl |
| TEMPONE | 4-oxo-2,2,6,6-teramethyl piperidin-1-oxyl |
| Tg | glass transition temperature |
| TMP–OH | 2,2,6,6-tetramethyl-4-piperidinol |
| TNF-α | tumor necrosis factor-α |

| | |
|---|---|
| Tsx | receptor protein for the phage T6 and colicin K |
| UV | ultra violet |
| $V_{max}$ | limiting rate |
| °C | degree Celsius |
| $[E_0]$ | enzyme concentration (at time zero) |
| [S] | Substrate concentration |

## Acknowledgements

This thesis would not have been possible with the help of many people. Therefore I would like express my cordially gratitude to all who contributed to this work.

I am very grateful to Prof. Wolfgang Meier for the possibility to be part of his research team. Equally thankful I am to Prof. Cornelia Palivan for giving my valuable inputs for my projects and Prof. Marcus Textor to be the co-refere

A special thank goes to Ozana Fischer-Onaca, who supported my during my PhD time as mentor and gave a lot of valuable knowledge. Furthermore I thank PD.Dr. Andrzej Sienkiewicz helping me to establish my first ESR experiment. I also would like to thank Stefan Egli, who synthesized during his PhD time the polymer I mainly used for my experiments. I also greatly acknowledge Vimalkumar Balasubramania introducing me in mammalian cell culturing. Many thanks go to Gaby Persy for the TEM measurements. Mariana Spulber I grateful thank, helping me doing ESR measurements and fruitful discussions. Additionally I thank Karolina Langowska helping me as new PhD student to get used with many equipment's and techniques I used during my time at the University of Basel.

Additionally, I thank to Gesine Gunkel and Marc Creus for proofreading my thesis

Many people have joined or left the group of Prof. Wolfgang Meier and Prof. Palivan while my graduation. I thank all of them for the friendly atmosphere and the excellent collaboration we had within the group.

I also gratefully acknowledging the students I worked with.

Without the finical support of the Swiss National Foundation (NRP 62) this PhD work would not had been possible, which is gratefully acknowledged.

# References


(1) Freitas, R. A. *Dm Disease-a-Month* **2005**, *51*, 325.

(2) Juliano, R. *Nature Reviews Drug Discovery* **2013**, *12*, 171.

(3) Boisseau, P.; Loubaton, B. *Comptes Rendus Physique* **2011**, *12*, 620.

(4) Boulaiz, H.; Alvarez, P. J.; Ramirez, A.; Marchal, J. A.; Prados, J.; Rodriguez-Serrano, F.; Peran, M.; Melguizo, C.; Aranega, A. *International Journal of Molecular Sciences* **2011**, *12*, 3303.

(5) Kim, K. T.; Meeuwissen, S. A.; Nolte, R. J. M.; van Hest, J. C. M. *Nanoscale* **2010**, *2*, 844.

(6) Chow, E. K.-H.; Ho, D. *Science Translational Medicine* **2013**, *5*.

(7) Lammers, T.; Hennink, W. E.; Storm, G. *British Journal of Cancer* **2008**, *99*, 392.

(8) IUPAC.

(9) IUPAC.

(10) Mai, Y.; Eisenberg, A. *Chemical Society Reviews* **2012**, *41*, 5969.

(11) Letchford, K.; Burt, H. *European Journal of Pharmaceutics and Biopharmaceutics* **2007**, *65*, 259.

(12) Lee, J. S.; Feijen, J. *Journal of Controlled Release* **2012**, *161*, 473.

(13) Rodriguez-Garcia, R.; Mell, M.; Lopez-Montero, I.; Netzel, J.; Hellweg, T.; Monroy, F. *Soft Matter* **2011**, *7*, 1532.

(14) Goddard, P.; Hutchinson, L. E.; Brown, J.; Brookman, L. J. *Journal of Controlled Release* **1989**, *10*, 5.

(15) Ruggiero, A.; Villa, C. H.; Bander, E.; Rey, D. A.; Bergkvist, M.; Batt, C. A.; Manova-Todorova, K.; Deen, W. M.; Scheinberg, D. A.; McDevitt, M. R. *Proceedings of the National Academy of Sciences of the United States of America* **2010**, *107*, 12369.

(16) Konradi, R.; Pidhatika, B.; Muehlebach, A.; Textort, M. *Langmuir* **2008**, *24*, 613.

(17) Immordino, M. L.; Dosio, F.; Cattel, L. *International Journal of Nanomedicine* **2006**, *1*, 297.

(18) Hoogenboom, R. *Angewandte Chemie-International Edition* **2009**, *48*, 7978.

(19) Viegas, T. X.; Bentley, M. D.; Harris, J. M.; Fang, Z.; Yoon, K.; Dizman, B.; Weimer, R.; Mero, A.; Pasut, G.; Veronese, F. M. *Bioconjugate Chemistry* **2011**, *22*, 976.

(20) Egli, S.; Fischer, B.; Hartmann, S.; Hunziker, P.; Meier, W.; Rigler, P. In *Modern Trends in Polymer Science-Epf 09*; Stelzer, F., Wiesbrock, E., Eds. 2010; Vol. 296, p 278.

(21) Zhang, C.; Xu, Y.; Zhong, Q.; Li, X.; Gao, P.; Feng, C.; Chu, Q.; Chen, Y.; Liu, D. *Plos One* **2014**, *9*.

(22) Yadollahi, R.; Vasilev, K.; Prestidge, C. A.; Simovic, S. *Journal of Nanomaterials* **2013**.

(23) Kaneda, Y.; Tsutsumi, Y.; Yoshioka, Y.; Kamada, H.; Yamamoto, Y.; Kodaira, H.; Tsunoda, S.; Okamoto, T.; Mukai, Y.; Shibata, H.; Nakagawa, S.; Mayumi, T. *Biomaterials* **2004**, *25*, 3259.

(24) Bélanger, M.-C.; Marois, Y. *Journal of Biomedical Material Research* **2001**, *58*, 11.

(25) Hua, F.; Sun, Y. G.; Gaur, A.; Meitl, M. A.; Bilhaut, L.; Rotkina, L.; Wang, J. F.; Geil, P.; Shim, M.; Rogers, J. A.; Shim, A. *Nano Letters* **2004**, *4*, 2467.

(26) Prinos, J.; Panayiotou, C. *Polymer* **1995**, *36*, 1223.

(27) Bellas, V.; Iatrou, H.; Hadjichristidis, N. *Macromolecules* **2000**, *33*, 6993.

(28) Yilgor, I.; McGrath, J. E. *Advances in Polymer Science* **1988**, *86*, 1.

(29) Yilgor, I.; Steckle, W. P.; Yilgor, E.; Freelin, R. G.; Riffle, J. S. *Journal of Polymer Science Part a-Polymer Chemistry* **1989**, *27*, 3673.

(30) Discher, D. E.; Eisenberg, A. *Science* **2002**, *297*, 967.

(31) Blanazs, A.; Armes, S. P.; Ryan, A. J. *Macromolecular Rapid Communications* **2009**, *30*, 267.

(32) Caruso, F. *Colloids and Colloid Assemblies*; Wiley-VCH GmbH ¬ Co. KGaA, 2004.

(33) Discher, D. E.; Ahmed, F. In *Annual Review of Biomedical Engineering* 2006; Vol. 8, p 323.

(34) Brinkhuis, R. P.; Rutjes, F. P. J. T.; van Hest, J. C. M. *Polymer Chemistry* **2011**, *2*, 1449.

(35) Lee, J. C. M.; Bermudez, H.; Discher, B. M.; Sheehan, M. A.; Won, Y. Y.; Bates, F. S.; Discher, D. E. *Biotechnology and Bioengineering* **2001**, *73*, 135.

(36) LoPresti, C.; Lomas, H.; Massignani, M.; Smart, T.; Battaglia, G. *Journal of Materials Chemistry* **2009**, *19*, 3576.

(37) Itel, F.; Chami, M.; Najer, A.; Loercher, S.; Wu, D.; Dinu, I. A.; Meier, W. *Macromolecules* **2014**, *47*, 7588.

(38) Najer, A.; Wu, D.; Vasquez, D.; Palivan, C. G.; Meier, W. *Nanomedicine* **2013**, *8*, 425.

(39) Chang, H.-I.; Yeh, M.-K. *International Journal of Nanomedicine* **2012**, *7*, 49.

(40) Allen, T. M.; Cullis, P. R. *Advanced Drug Delivery Reviews* **2013**, *65*, 36.

(41) Li, W. *Trends In Bio/Pharmaceuti cal Industry* **2006**, *3*, 5.

(42) Fenske, D. B.; Cullis, P. R. *Expert Opinion on Drug Delivery* **2008**, *5*, 25.

(43) Li, S.; Byrne, B.; Welsh, J.; Palmer, A. F. *Biotechnology Progress* **2007**, *23*, 278.

(44) Murdoch, C.; Reeves, K. J.; Hearnden, V.; Colley, H.; Massignani, M.; Canton, I.; Madsen, J.; Blanazs, A.; Armes, S. P.; Lewis, A. L.; MacNeil, S.; Brown, N. J.; Thornhill, M. H.; Battaglia, G. *Nanomedicine* **2010**, *5*, 1025.

(45) Balasubramanian, V.; Onaca, O.; Enea, R.; Hughes, D. W.; Palivan, C. G. *Expert Opinion on Drug Delivery* **2010**, *7*, 63.

(46) Axthelm, F.; Casse, O.; Koppenol, W. H.; Nauser, T.; Meier, W.; Palivan, C. G. *Journal of Physical Chemistry B* **2008**, *112*, 8211.

(47) Spulber, M.; Baumann, P.; Saxer, S. S.; Pieles, U.; Meier, W.; Bruns, N. *Biomacromolecules* **2014**, *15*, 1469.

(48) Renggli, K.; Baumann, P.; Langowska, K.; Onaca, O.; Bruns, N.; Meier, W. *Advanced Functional Materials* **2011**, *21*, 1241.

(49) Langowska, K.; Palivan, C. G.; Meier, W. *Chemical Communications* **2013**, *49*, 128.

(50) Tanner, P.; Balasubramanian, V.; Palivan, C. G. *Nano Letters* **2013**, *13*, 2875.

(51) Baumann, P.; Balasubramanian, V.; Onaca-Fischer, O.; Sienkiewicz, A.; Palivan, C. G. *Nanoscale* **2013**, *5*, 217.

(52) Stauch, O.; Schubert, R.; Savin, G.; Burchard, W. *Biomacromolecules* **2002**, *3*, 565.

(53) www.wikipedia.org

(54) Master, A.; Livingston, M.; Sen Gupta, A. *Journal of Controlled Release* **2013**, *168*, 88.

(55) Dolmans, D.; Fukumura, D.; Jain, R. K. *Nature Reviews Cancer* **2003**, *3*, 380.

(56) Henderson, B. W.; Dougherty, T. J. *Photochemistry and Photobiology* **1992**, *55*, 145.

(57) Almeida, R. D.; Manadas, B. J.; Carvalho, A. P.; Duarte, C. B. *Biochimica Et Biophysica Acta-Reviews on Cancer* **2004**, *1704*, 59.

(58) Celli, J. P.; Spring, B. Q.; Rizvi, I.; Evans, C. L.; Samkoe, K. S.; Verma, S.; Pogue, B. W.; Hasan, T. *Chemical Reviews* **2010**, *110*, 2795.

(59) Barolet, D. *Seminars in Cutaneous Medicine and Surgery* **2008**, *27*, 227.

(60) Mroz, P.; Yaroslavsky, A.; Kharkwal, G. B.; Hamblin, M. R. *Cancers* **2011**, *3*, 2516.

(61) Sadasivam, M.; Avci, P.; Gupta, G. K.; Lakshmanan, S.; Chandran, R. H., Y.; M.R., K. R. H. *Eur. J. Nanomed* **2013**, *5*, 15.

(62) Fang, J.; Nakamura, H.; Maeda, H. *Advanced Drug Delivery Reviews* **2011**, *63*, 136.
(63) Mathai, S.; Smith, T. A.; Ghiggino, K. P. *Photochemical & Photobiological Sciences* **2007**, *6*, 995.
(64) Chang, C.-C.; Yang, Y.-T.; Yang, J.-C.; Wu, H.-D.; Tsai, T. *Dyes and Pigments* **2008**, *79*, 170.
(65) Tseng, S. C. G.; Feenstra, R. P. G.; Watson, B. D. *Investigative Ophthalmology & Visual Science* **1994**, *35*, 3295.
(66) Abuin, E.; Aspée, A.; Leon, L. *J. Chil. Chem. Soc* **2007**, *52*.
(67) Nardin, C.; Thoeni, S.; Widmer, J.; Winterhalter, M.; Meier, W. *Chemical Communications* **2000**, 1433.
(68) Harabagiu, V.; Hamciuc, V.; Giurgiu, D.; Simionescu, B. C.; Simionescu, C. I. *Makromolekulare Chemie-Rapid Communications* **1990**, *11*, 433.
(69) Baumann, P.; Spulber, M.; Dinu, I. A.; Palivan, C. G. *Journal of Physical Chemistry B* **2014**, *118*, 9361.
(70) Kumar, M.; Grzelakowski, M.; Zilles, J.; Clark, M.; Meier, W. *Proceedings of the National Academy of Sciences of the United States of America* **2007**, *104*, 20719.
(71) Tanner, P.; Balasubramanian, V.; Onaca, O.; Meier, W.; Palivan, C. G. *Abstracts of Papers of the American Chemical Society* **2012**, *243*.
(72) Litvinchuk, S.; Lu, Z.; Rigler, P.; Hirt, T. D.; Meier, W. *Pharmaceutical Research* **2009**, *26*, 1711.
(73) Langowska, K.; Kowal, J.; Palivan, C. G.; Meier, W. *Journal of Materials Chemistry B* **2014**, *2*, 4684.
(74) Masters, J. R. *Nature Reviews Cancer* **2002**, *2*, 315.
(75) Mousavi, S. H.; Tavakkol-Afshari, J.; Brook, A.; Jafari-Anarkooli, I. *Food and Chemical Toxicology* **2009**, *47*, 855.
(76) Youssef, T.; Kassem, M.; Abdella, T.; Harith, M. A.; Lenci, F. *Photochemistry and Photobiology* **2009**, *85*, 1306.
(77) Wu, C.; Wu, Y.-H. *Biochemistry* **1973**, *12*, 7.
(78) Shang, L.; Nienhaus, K.; Nienhaus, G. U. *Journal of Nanobiotechnology* **2014**, *12*.
(79) Sakai, N.; Matsui, Y.; Nakayama, A.; Tsuda, A.; Yoneda, M. *Journal of Physics :Conference Series* **2011**, *304*, 10.
(80) Hood, R. R.; Andar, A.; Omiatek, D. M.; Vreeland, W. N.; Swaan, P. W.; DeVoe, D. L. *16th International Conference on Miniaturized Systems for Chemistry and Life Sciences* **2012**, 3.
(81) Barenholz, Y. *Journal of Controlled Release* **2012**, *160*, 117.
(82) Tacar, O.; Sriamornsak, P.; Dass, C. R. *Journal of Pharmacy and Pharmacology* **2013**, *65*, 157.
(83) Tian, B.; Wang, C.; Zhang, S.; Feng, L.; Liu, Z. *Acs Nano* **2011**, *5*, 7000.
(84) Horfelt, C.; Funk, J.; Frohm-Nilsson, M.; Edstrom, D. W.; Wennberg, A. M. *British Journal of Dermatology* **2006**, *155*, 608.
(85) Dougherty, T. J.; Gomer, C. J.; Henderson, B. W.; Jori, G.; Kessel, D.; Korbelik, M.; Moan, J.; Peng, Q. *Journal of the National Cancer Institute* **1998**, *90*, 889.
(86) Cornish-Bowden, A. *Fundamentals of Enzyme Kinetics*; 4th ed.; Wiley-Blackwell, 2012.
(87) Veitch, N. C. *Phytochemistry* **2004**, *65*, 249.
(88) Voepel, T.; Makhatadze, G. I. *Plos One* **2012**, *7*.
(89) Pitulice L; Pastor I; Vilaseca E; Madurga S; A, I. *J Biocatal Biotransformation* **2013**, *2*.
(90) Ellis, R. J. *Trends in Biochemical Sciences* **2001**, *26*, 597.
(91) Zimmerman, S. B.; Trach, S. O. *Journal of Molecular Biology* **1991**, *222*, 599.
(92) Kunkel, J.; Asuri, P. *Plos One* **2014**, *9*.

(93) Housden, N. G.; Wojdyla, J. A.; Korczynska, J.; Grishkovskaya, I.; Kirkpatrick, N.; Brzozowski, A. M.; Kleanthous, C. *Proceedings of the National Academy of Sciences of the United States of America* **2010**, *107*, 21412.

(94) Koebnik, R.; Locher, K. P.; Van Gelder, P. *Molecular Microbiology* **2000**, *37*, 239.

(95) Mecke, A.; Dittrich, C.; Meier, W. *Soft Matter* **2006**, *2*, 751.

(96) Zhou, L.; Schlick, S. *Polymer* **2000**, *41*, 4679.

(97) Nakagawa, K. *Lipids* **2007**, *42*, 457.

(98) Beghein, N.; Rouxhet, L.; Dinguizli, M.; Brewster, M. E.; Arien, A.; Preat, V.; Habib, J. L.; Gallez, B. *Journal of Controlled Release* **2007**, *117*, 196.

(99) Sengupta, P.; Garai, K.; Balaji, J.; Periasamy, N.; Maiti, S. *Biophysical Journal* **2003**, *84*, 1977.

(100) Rigler, P.; Meier, W. *Journal of the American Chemical Society* **2006**, *128*, 367.

(101) Onaca, O.; Hughes, D. W.; Balasubramanian, V.; Grzelakowski, M.; Meier, W.; Palivan, C. G. *Macromolecular Bioscience* **2010**, *10*, 531.

(102) Tanner, P.; Onaca, O.; Balasubramanian, V.; Meier, W.; Palivan, C. G. *Chemistry-a European Journal* **2011**, *17*, 4552.

(103) Glettenberg, M.; Niemeyer, C. M. *Bioconjugate Chemistry* **2009**, *20*, 969.

(104) Norris, M. G. S.; Malys, N. *Biochemical and Biophysical Research Communications* **2011**, *405*, 388.

(105) Zabara, A.; Negrini, R.; Baumann, P.; Onaca-Fischer, O.; Mezzenga, R. *Chemical Communications* **2014**, *50*, 2642.

(106) Nallani, M.; Benito, S.; Onaca, O.; Graff, A.; Lindemann, M.; Winterhalter, M.; Meier, W.; Schwaneberg, U. *Journal of Biotechnology* **2006**, *123*, 50.

(107) Fruk, L.; Mueller, J.; Niemeyer, C. M. *Chemistry-a European Journal* **2006**, *12*, 7448.

# Patric Baumann

Jägerstrasse 12 • 4058 Basel • 079 288 24 33 • Patric.Baumann@unibas.ch

## EDUCATION:

**University of Basel**, Department of Chemistry and Swiss Nanoscience Institute, Basel, Switzerland

- PhD in Nanoscience, March 2015
- Master in Nanoscience, Major in Chemistry, March 2010
- Bachelor in Nanoscience, June 2008

## RESEARCH EXPERIENCE:

**Novartis Pharma AG, Basel, Technical Research and Development**
**Postodoctoral Candiated in Nanomedicine**, Nanomedicine Platform 2014 - present

- Screening and optimizing of liposome formulation for intracellular delivery and sustained release.
- Solubilization of drug substance in liposome and stability measurements.
- Optimizing and up-scaling of different liposome manufacturing techniques to test possibilities for GMP production.

**University of Basel, Department of Chemistry**
**Scientific Associate** with Prof. Dr. W. Meier and Prof. Dr. C. Palivan, 2010 – 2014

- Studied the self-assembly behaviour of amphiphilic block copolymers into polymersome structures and prepare them for medical and therapeutic applications.
- Reconstituted membrane protein into polymeric membranes to make them permeable for specific molecules.
- Encapsulated enzymes in so called nanoreactors to enhance their stability and activity.
- Used mammalian cells to test drug delivery potential for polymersome formulations.

**University of Basel, Department of Chemistry**
**Scientific Associate** with Prof. Dr. W. Meier and Dr. O. Fischer, 2009 – 2010

- Master thesis focused on screening for different enzymes and substrates pairs to form nanoreactors and measuring their activity.

**University of Basel, Biozentrum**
**Scientific Associate** with Prof. Dr. D. Klostermeier, spring 2009

- Project work on total internal reflection fluorescence microscopy to detect single fluorescence resonance energy transfer pairs in immobilized liposomes.

## SKILLS AND ADDITIONAL INFORMATION:

- **Laboratory and equipment skills:**
  Particle size measurement, HPLC, Formulation screening, Isothermal titration calorimetry, Chromatography, Transmissions electron microscopy, Fluorescence and UV-Vis microscopy, Polymersome and liposome formation**,** Mammalian and bacterial cell culture, Confocal laser scanning microscopy, Expression, purification and characterization of proteins, Cell based assays for viability and ROS determination, Flow cytometry, Genetic manipulation and labelling of membrane proteins

- **Management skills:**
  Responsible for microbiological laboratory including lab cleaning, safety, purchasing and instrument maintenance.

- **Teaching Assistant**, University of Basel, Department of Chemistry
  Supervised a master student by introducing him to the lab work and trained him on several instruments. Regular scientific problem discussion and progress evaluation.
  Directly supervised and trained undergraduate students in research experiments and corrected and reviewing their reports.
  Conducted laboratory classes in physical chemistry by introducing to the experiments and corrected the student's reports. Prepared and corrected exam sets.

- **Languages:**
  German – native, English – fluent, French – advanced

- **IT skills:**
  Operating Program: Windows, OS X, iOS
  Office Program: MS Office, OpenOffice
  Instruments Software: Chromeleon, Carl Zeiss LSM software ConfoCor, PrimeView, FL WinLab, NANODROP 2000/2000c, SoftMax Pro, ImageLab,
  Others: eLN, Corel Draw, ChemDraw, GIMP, Origin, EndNote, LabVIEW, Minitab

- **Activities:**
  Active Member of the Chemistry Department Conference, 2011- present
  Member of the organizing committee of the Science Slam Basel, 2011- present
  Member of the organizing committee of the PolyColl Basel, 2013

## SELECTED PUBLICATIONS:


- P. Baumann, M. Spulber, I. A. Dinu, C. G. Palivan
  Cellular Trojan Horse Based Polymer Nanoreactors with Light-Sensitive Activity
  Physical Chemistry B, 2014, 118, 9361

- M. Spulber, P. Baumann, S. S. Saxer, U. Pieles, W. Meier, N. Bruns
  Poly(*N*-vinylpyrrolidone)-Poly(dimethylsiloxane)-Based Polymersomes Nanoreactors for Laccase-Catalyzed Biotransformations
  Biomacromolecules, 2014, 15, 1469

- D. Vasquez, R. Milusheva, P. Baumann, D. Constantin, M. Chami, C. G. Palivan
  The Amine content of PEGylated Chitosan *Bombyx morin* Nanoparticles Acts as a Trigger for Protein Delivery
  Langmuir, 2014, 30, 965

- P. Baumann, V. Balasubramanian, O. Onaca-Fischer, A. Sienkiewicz, C. Palivan
  Light- responsive polymer nanoreactors: a source of reactive oxygen species on demand
  Nanoscale, 2013, 5, 217

- K. Renggli, P. Baumann, K. Langowska, O. Onaca, N. Bruns, W. Meier
  Selective and Responsive Nanoreactors
  Advanced Functional Materials, 2011, 21, 1241

- P. Baumann, P. Tanner, O. Onaca, C. Palivan, W. Meier
  Bio-Decorated Polymer Membranes: A new Approach in Diagnostic and Therapeutics
  Polymers, 2011, 3, 173